BOREAS An international journal of Quaternary research

Hässeldala – a key site for Last Termination climate events in northern Europe

1   Hässeldala – a key site for Last Termination climate events in

2   northern Europe

3

4   BARBARA WOHLFARTH, FRANCESCO MUSCHITIELLO, SARAH GREENWOOD,

5   AUGUST ANDERSSON, MALIN KYLANDER, RIENK H. SMITTENBERG, MARGRET

6   STEINTHORSDOTTIR, JENNY WATSON AND NICOLA J. WHITEHOUSE

7

11

12

13   The Last Termination (19 000-11 000 a BP) with its rapid and distinct climate

14   shifts provides a perfect laboratory to study the nature and regional impact of

15   climate variability. The sedimentary succession from the ancient lake at

16   Hässeldala Port in southern Sweden with its distinct Lateglacial/early Holocene

17   stratigraphy (>14.1-9.5 cal. ka BP) is one of the few chronologically well-

18   constrained, multi-proxy sites in Europe that capture a variety of local and

19   regional climatic and environmental signals. Here we present Hässeldala's multi-

20   proxy records (lithology, geochemistry, pollen, diatoms, chironomids,

21   biomarkers, hydrogen isotopes) in a refined age model and place the observed

22   changes in lake status, catchment vegetation, summer temperatures and

23   hydroclimate in a wider regional context. Reconstructed mean July temperatures

24   increased between ~14.1 and ~13.1 cal. ka BP and subsequently declined. This

25   latter cooling coincided with drier hydroclimatic conditions that were likely

26   associated with a freshening of the Nordic Seas and started a few hundred years

27   before the onset of Greenland Stadial 1 (~12.9 cal. ka BP). Our proxies suggest a

28   further shift towards colder and drier conditions as late as ~12.7 cal. ka BP,

29   which was followed by the establishment of a stadial climate regime (~12.5-11.8

30   cal. ka BP). The onset of warmer and wetter conditions led the Holocene

31   warming over Greenland by ~200 years. Hässeldala's proxies thus highlight the

32   complexity of environmental and hydrological responses across abrupt climate

33   transitions in northern Europe.

34

Barbara Wohlfarth (barbara.wohlfarth@geo.su.se), Francesco Muschitiello, Sarah Greenwood, Malin Kylander, Rienk H. Smittenberg and Margret Steinthorsdottir, Department of Geological Sciences and Bolin Centre for Climate Research, Stockholm University, SE-10691, Stockholm, Sweden; August Andersson, Department of Applied Environmental Science and Bolin Centre for Climate Research, Stockholm University, SE-10691, Stockholm, Sweden; Jenny Watson, School of Geography, Archaeology and Palaeoecology, Queen's University Belfast, Belfast BT7 1NN, UK; Nicola J. Whitehouse, School of Geography, Earth and Environmental Sciences, Plymouth University, Drake Circus, Plymouth PL4 8AA, United Kingdom; received 18th May 2016, accepted 18th August 2016.

45

The transition period from the Last Glacial Maximum into the present Interglacial (the Holocene) occurred between 19 and 11 thousand years (ka) before present (BP) and is informally known as the 'Last Deglaciation' or the 'Last Termination'. This interval is characterised by a series of abrupt climate shifts of colder (stadial) and warmer (interstadial) states, which are most prominently expressed in the North Atlantic region (Björck *et al.* 1996; Lowe *et al.* 2008; Steffensen *et al.* 2008). These stadials and interstadials are often referred to as 'Oldest Dryas' (>14.7 ka BP), 'Bølling' (14.7-14.1 ka BP), 'Older Dryas' (14.1-13.9 ka BP), 'Allerød' (14.1-12.9 ka BP) and 'Younger Dryas' (12.9-11.7 ka BP) (Rasmussen *et al.* 2014) in reference to earlier pollen-stratigraphic work in Scandinavia (see e.g. Mangerud *et al.* 1974; Wohlfarth 1996).

Greenland ice core records have played a pivotal role in understanding the underlying causes of abrupt deglacial climate variability, because they (i) record climate shifts in a multitude of atmospheric proxies (Steffensen *et al.* 2008); (ii) provide a precise chronological template for past climatic events (Rasmussen *et al.* 2014); and (iii) can be synchronized to Antarctic ice cores using methane measurements (Blunier & Brook 2001). This synchronization allows for a direct correlation of Northern and Southern Hemisphere climatic changes and supports the hypothesis of the Atlantic bipolar seesaw concept (Broecker 1998), which attributes a large role to the Atlantic Meridional Overturning Circulation in triggering abrupt climate shifts (Stocker & Johnsen 2003; Knutti *et al.* 2004; EPICA 2006). The INTIMATE working group thus proposed to use the Greenland ice core isotope stratigraphy as a template

69   against which marine and terrestrial records could be compared to decipher

70   leads and lags between different regions (Björck *et al.* 1998; Walker *et al.* 1999).

71   Unfortunately, rather than using independent chronological information to

72   enable a critical appraisal of event sequences, many simply wiggle-matched their

73   respective proxy stratigraphies to the Greenland ice core oxygen isotope curve.

74   Lowe *et al.* (2008) and later Blockley *et al.* (2012) and Rasmussen *et al.* (2014)

75   therefore refined the INTIMATE event stratigraphy by including cryptotephra

76   layers that can be found in marine, ice core and terrestrial records and used as

77   time-synchronous marker horizons. This latter approach has clear advantages as

78   compared with simple wiggle-matching, but it soon became clear that a reliance

79   only on cryptotephra layers to correlate between sites can be misleading as the

80   ash may be reworked and/or originate from multiple eruptions of the same

81   volcano with similar geochemical signatures (see e.g. Davies *et al.* 2004; Pyne-

82   O'Donnell *et al.* 2008, 2010).

83   Although considerable advances have been made with respect to

84   cryptotephra studies (Lowe *et al.* 2015) and radiocarbon calibration (Reimer *et*

85   *al.* 2013), the lack of high-resolution, independent chronologies for terrestrial

86   and marine records still makes it impossible to compare the exact regional and

87   hemispheric phasing of Last Termination climatic events, albeit with a few

88   exceptions (Lane *et al.* 2013; Lohne *et al.* 2013, 2014; Muschitiello & Wohlfarth

89   2015; Rach *et al.* 2014; Muschitiello *et al.* 2015b). Moreover, the detection of

90   spatiotemporal differences of up to several hundred years in respect to

91   temperature, precipitation, and vegetation changes both at the start of (Rach *et*

92   *al.* 2014; Muschitiello & Wohlfarth 2015) and during Younger Dryas (Lane *et al.*

93   2013), suggests that the propagation of climatic signals on regional to sub-

94   continental scales is still not fully understood. The assumption of more or less

95   synchronous hydroclimatic and ecosystem responses even on regional scales is

96   therefore clearly an oversimplification.

97   While chronological uncertainties surely play a major role when

98   attempting to correlate between different archives (Blaauw 2012), the detection

99   of past environmental and climatic shifts in various terrestrial archives also very

100   much depends on (i) the choice of biological, chemical and physical proxies to be

101   studied and their respective environmental and climatic information (e.g.,

102 seasonal temperature, precipitation, windiness, run-off, aquatic and terrestrial

103 vegetation, lake status changes); (ii) understanding the complicated ecological

104 processes that drive biotic and abiotic changes (e.g. Jackson & Overpeck 2000;

105 Ammann *et al.* 2013; Birks & Birks 2014) and lake development (Engstrom *et al.*

106 2000); and (iii) the transfer functions and other methods used to derive

107 temperature estimates from micro- and macrofossil data sets (e.g. Juggins 2013;

108 Brooks & Langdon 2014).

109   The Last Termination, with its rapid and distinct climate shifts, is an

110 excellent time period to study the nature and regional impact of climate

111 variability. Few lake sedimentary successions in Europe however fulfil the

112 requirement of being chronologically well-constrained, multi-proxy sites that are

113 able to capture the variety of climatic and environmental signals preserved

114 within the fossil record and enable unequivocal comparisons to the Greenland

115 ice core template chronology (Ammann *et al.* 2013; Birks & Birks 2014; Rach *et*

116 *al.* 2014; Muschitiello & Wohlfarth 2015). One of these is the sedimentary

117 succession from the ancient lake at Hässeldala Port in southern Sweden (Fig 1A-

118 C), which displays a distinct Lateglacial stratigraphy (Davies *et al.* 2004). Since

119 the discovery of several cryptotephra layers in Hässeldala Port's sediments

120 (Davies *et al.* 2003), the site has been the focus of a variety of proxy studies, most

121 of which were performed on various parallel sediment cores (Davies *et al.* 2004;

122 Wohlfarth *et al.* 2006; Watson 2008; Kylander *et al.* 2013; Steinthorsdottir *et al.*

123 2013, 2014; Ampel *et al.* 2014; Muschitiello *et al.* 2015a, b; Karlatou-

124 Charalampopoulou 2016) (Fig. 1C, Table 1). Except for the most recent studies

125 (Steinthorsdottir *et al.* 2013; Ampel *et al.* 2014; Muschitiello *et al.* 2015b;

126 Karlatou-Charalampopoulou 2016), the chronology of core #2 and visual core-

127 to-core correlations were used (Davies *et al.* 2004; Wohlfarth *et al.* 2006; Watson

128 2008; Kylander *et al.* 2013). The latter approach was justified because total

129 organic carbon (TOC) and/or loss-on-ignition (LOI) measurements for each

130 analysed profile show the same characteristic pattern and allowed for a direct

131 correlation between parallel sediment cores and their lithostratigraphic units

132 (Wohlfarth *et al.* 2006).

133   Alignment of the various parallel profiles using a Monte Carlo based

134 approach and the most recent and updated age model for core #5 (Muschitiello

135   *et al.* 2015b) now offer the possibility to present the suite of proxy records for

136   Hässeldala Port on one common time scale and to discuss local and regional

137   responses to Last Termination climate events. The different proxies analysed in

138   Hässeldala Port's sedimentary profiles have been described in detail in various

139   publications (see Table 1 for references), but except for the chironomid-based

140   temperature reconstruction and the biomarker data set, which have been

141   presented on an updated chronology (Muschitiello *et al.* 2015a, b), none of the

142   other proxies has been discussed within the context of the new chronology for

143   core #5. Here we combine Hässeldala Port's various sediment cores and proxies

144   and present these on the chronology for core #5 to discuss the timing and impact

145   of Lateglacial climatic shifts in southern Sweden and to address leads and lags

146   between changes in hydroclimate and vegetation across Europe.

147

148   Hässeldala Port - background

149   The ancient lake that existed during the Last Termination at Hässeldala Port

150   (56'16° N, 15'01° E; 63 m a.s.l.) in Blekinge province, southern Sweden (Fig. 1A-

151   C), filled in during the early Holocene. Today the site is a peat bog that is partly

152   covered by a mixed pine-birch forest, shrubs (*Juniperus*, Ericales), grass, mosses

153   and ferns. Peat has been excavated extensively during the first half of the 20th

154   century and Lateglacial sediments can therefore be found in a depth of less than

155   three meters. This, and the easy access to the site, has led to several coring

156   campaigns during the past fifteen years. Coring was always performed using a

157   Russian corer of 1 m length and 10 cm diameter.

158   Since Hässeldala Port's Lateglacial and early Holocene sediment

159   succession is contained within one meter of sediment, it precisely fits the length

160   of the coring chamber and can be recovered without the need of overlaps. The

161   deepest part of the basin was found to be in the south-western corner of the bog.

162   It is from this restricted area, where all analysed sediment cores have been

163   obtained (Fig. 1C, Table 1). The exact GPS location of each coring point has

164   however not been recorded and lithostratigraphic transects combining all

165   studied profiles are therefore not possible, other than those shown in Wohlfarth

166   *et al.* (2006).

167 The first to acknowledge the potential of Hässeldala Port's Lateglacial
168 sediments were Davies *et al.* (2003), who described five different cryptotephra
169 horizons from core #1 (Fig. 1C, Tables 1, 2). Of these three were correlated to
170 known eruptions based on their geochemical signatures: the Borrobol tephra
171 (BT), the newly defined Hässeldala tephra (HDT) and the Askja-S tephra (AsT)
172 (Table 2). Two tephras could not be correlated to any known eruption. Using the
173 pattern of the loss-on-ignition (LOI) curve of core #1, Davies *et al.* (2003)
174 tentatively assigned climatic/pollen stratigraphic periods and suggested that the
175 BT would date to the Bølling-Allerød Interstadial and the HDT and the AsT to the
176 early Holocene. However, the finding of two superimposed cryptotephras in
177 Lateglacial sediments in Scotland, which both seem to have been derived from
178 the same volcanic source, led Matthews *et al.* (2011) to suggest that Hässeldala
179 Port's BT is younger than the BT found in Scotland and likely an equivalent to the
180 Penifiler tephra.

181 Subsequent analyses were made on cores #2 (LOI, ^{14}C chronology) and #3
182 (TOC, cryptotephra, pollen stratigraphy) (Fig. 1C, Tables 1, 2) (Davies *et al.* 2004;
183 Andersson 2004; Wohlfarth *et al.* 2006). Both profiles showed an identical
184 stratigraphy and a good match between the LOI/TOC curves, which facilitated
185 visual inter-core correlations. The different age models established for core #2
186 were therefore transferred to core #3 and provided age estimates for the three
187 geochemically identified cryptotephra layers of 14.3-13.7 cal. ka BP ('BT'), 11.6-
188 11.2 cal. ka BP (HDT) and 11.1-10.6 cal. ka BP (AsT) (Wohlfarth *et al.* 2006). The
189 reconstructed vegetation development showed that arctic and sub-arctic plant
190 species dominated during the Lateglacial and that *Pinus sylvestris* and *Betula*
191 *pubescens* were present at the transition between the Younger Dryas and
192 Preboreal pollen zones (Andersson 2004; Wohlfarth *et al.* 2006). Moreover,
193 approximate ages for the regional Lateglacial pollen zone boundaries were
194 established using a suite of different age models. These suggested ages of 14.2-
195 13.7 cal. ka BP for the Older Dryas/Allerød pollen zone transition, of 13.1-12.6
196 cal. ka BP for the Allerød/Younger Dryas transition and of 11.9-11.3 cal. ka BP
197 for the Younger Dryas/Preboreal transition (Wohlfarth *et al.* 2006).

198 A set of twelve new sediment cores were later obtained by Watson
199 (2008), analysed for LOI, cryptotephra, Coleoptera and chironomids (Fig. 1C,

200   Tables 1, 2) and correlated to cores #2 and #3. Six of these profiles were

201   subsampled and aggregated for Coleoptera analysis; LOI analyses were

202   undertaken on four cores to aid cross-core correlation (#HP4, #HP6, #HP9,

203   #HP12) and chironomids were analysed from core #HP4 (Fig. 1C, Table 1).

204   Cryptotephra was found in core #HP4 and was tentatively correlated to core #1

205   using the pattern of the LOI curve (Watson 2008) (Table 2). The Coleoptera

206   assemblages, which represent mean summer air temperatures, suggested mild

207   and cool summers until about 13.4 cal. ka BP with reconstructed mean summer

208   temperatures of about 14 °C (Watson 2008). At the Younger Dryas/Holocene

209   transition, Coleoptera, which are typical of acid bog environments and dry shrub

210   heathland such as *Amara alpina* and *Olophrum boreale*, appear suggesting a

211   change in lake status. The chironomid assemblages also show clear shifts in

212   species composition and point to a shift from oligotrophic to increasingly

213   eutrophic lake water conditions (Watson 2008). Moreover, the chironomid

214   assemblages allowed reconstructing mean summer surface water temperatures

215   between *c.* 14.2 and 11.8 cal. ka BP in great detail (Watson 2008; Muschitiello *et*

216   *al.* 2015b).

217   Kylander *et al.* (2013) analysed the geochemistry in core #4 (Fig. 1C,

218   Table 1) and, using lithostratigraphic markers and the TOC curve, matched this

219   profile to cores #2 and #3 to obtain a general chronostratigraphic framework.

220   Higher sediment accumulation rates were reconstructed for the pre-Allerød

221   period, while a relative constant sediment supply seems to have characterised

222   the Allerød and Younger Dryas pollen zones.

223   The most recent investigations focussed on core #5 (Fig. 1C) and

224   provided a new chronology and age model, an atmospheric CO_2 reconstruction

225   using leaf stomata (Steinthorsdottir *et al.* 2013, 2014), lake status changes based

226   on diatom assemblages (Ampel *et al.* 2014) and geochemistry (Muschitiello *et al.*

227   2015a) and a hydroclimate reconstruction using lipid biomarkers (Muschitiello

228   *et al.* 2015b). These latter analyses were based on hydrogen isotopes derived

229   from aquatic (n-C_{21}) and terrestrial (n-$C_{27-29-31}$) alkanes and can be used as

230   proxies for moisture source composition and terrestrial evaporation

231   (Muschitiello *et al.* 2015b) (Table 1). All sub-samples were taken in 1 cm

232   increments along core #5 and split to accommodate various proxy analyses.

233   However, to provide enough leaf material for stomatal analyses, several parallel

234   cores had to be sub-sampled after precise lithostratigraphic correlation to the

235   master core #5 (Steinthorsdottir *et al.* 2013, 2014). Lastly, a new high-resolution

236   pollen stratigraphy, combined with LOI measurements, was established on parts

237   of core #6 (Muschitiello *et al.* 2015b; Karlatou-Charalampopoulou 2016) (Fig. 1C,

238   Table 1).

239   Although the lithostratigraphy and the LOI/TOC curves for the parallel

240   profiles facilitated visual core-to-core correlations (Wohlfarth *et al.* 2006), this

241   eyeballing exercise did not allow for a precise transfer of proxy data from one

242   core to another. Muschitiello *et al.* (2015b) therefore statistically aligned cores

243   #2, #HP4, #5 and #6 with each other. This made it possible to update the

244   existing chronology for core #5 and provided a possibility to discuss climate

245   responses across the Allerød/Younger Dryas pollen zone transition in greater

246   detail (Muschitiello *et al.* 2015b).

247

248   Lithostratigraphy and core-to-core correlations

249   Hässeldala Port's sediment cores are all derived from the southwestern part of

250   the peatbog (Fig. 1C) and display an almost identical lithostratigraphic

251   succession, which is also reflected in the respective TOC/LOI curves (Davies *et al.*

252   2003, 2004; Wohlfarth *et al.* 2006; Kylander *et al.* 2013; Steinthorsdottir *et al.*

253   2013, 2014; Karlatou-Charalampopoulou 2016). Since the bottom topography of

254   the bog is not even, the depth of the Lateglacial/early Holocene profiles varies

255   slightly, as does the thickness of individual layers (Wohlfarth *et al.* 2006) (Figs 2,

256   3A). Despite this, the recovered Lateglacial/early Holocene successions show a

257   distinct and repetitive lithostratigraphic pattern (Figs 2, 3A): the bottommost

258   sediments in all cores are composed of grey silty sand and clayey silt/silty clay

259   (units 1 and 2) with low organic matter content; higher, but variable LOI/TOC

260   values characterise the silty clay gyttja and/or clay gyttja layers of units 3 to 6

261   (Fig. 2); and the dark brown silty clayey gyttja/clayey gyttja of unit 7 with its

262   high LOI/TOC values is distinct in all profiles, as is the overlying greenish-

263   brown/brown clayey gyttja of unit 8 with its markedly lower LOI/TOC values

264 (Wohlfarth *et al.* 2006) (Fig. 2). The sediments in the uppermost part are made

265 up of clay gyttja, gyttja and peaty gyttja (units 9-12) with high LOI/TOC values.

266 Lithostratigraphic core-to-core correlations are thus straightforward and

267 are also supported by the very similar pattern of the accompanying LOI/TOC

268 curves (Figs 2, 3A). These display the same characteristic features in all six

269 sequences with low organic contents in the bottommost part, gradually rising,

270 but variable TOC/LOI values, a distinct peak in organic content, a decrease in

271 LOI/TOC values and subsequent high values (Fig. 3A). However visual core-to-

272 core correlations or visual curve matching do not allow transferring proxies

273 from one sediment core to another or projecting the various proxies on the new

274 chronology of core #5. We therefore follow the approach presented in

275 Muschitiello *et al.* (2015a, b), who used a Monte Carlo Markov Chain algorithm

276 for core-to-core alignment. This method provides a suite of possible alignments

277 between stratigraphic series and the target series and estimates the optimal

278 correlation (see Muschitiello *et al.* 2015b for further details). For Hässeldala

279 Port, we use the high-resolution LOI/TOC curves of cores #1-3, HP4 and 6 as

280 stratigraphic series and the LOI curve of core #5 as target series (Fig. 3A). Prior

281 to the statistical analyses, the TOC values of cores #1, 2 and 3 were recalculated

282 to LOI values to facilitate the statistical correlation. The alignment of the LOI

283 curves of cores #1-3, HP4 and 6 to the LOI curve of core #5 then provided a

284 means to transfer the plant macrofossil record and the ^{14}C dates of core #2, the

285 pollen stratigraphy of core #3 (Wohlfarth *et al.* 2006), the chironomid-based

286 summer temperature reconstruction of core #HP4 (Watson 2008) and the high-

287 resolution pollen stratigraphy of core #6 (Karlatou-Charalampopoulou 2016) to

288 the stratigraphy of core #5 (Muschitiello *et al.* 2015b). However, since the

289 chironomid data set of core #HP4 had a higher temporal sampling resolution

290 than samples taken from core #5, the data set had to be interpolated to the

291 sampling resolution of master core #5 (Muschitiello *et al.* 2015b).

292

293 Age-depth model and chronology

294

295 Using the same core-to-core alignment approach as outlined above, Muschitiello

296 *et al.* (2015b) updated the earlier age model for core #5 (Steinthorsdottir *et al.*

297 2013, 2014) by transferring the ^{14}C dates from core #2 to the stratigraphy of

298 core #5 (Table 3, Fig. 4).

299   Age-depth curves were constructed (Muschitiello *et al.* 2015b) using

300 Bacon2.2. (Blaauw & Christen 2011) and OxCal4.2 (Bronk Ramsey 2010) after

301 calibration with IntCal13 (Reimer *et al.* 2013). Since both age models provided

302 very similar results, we here use OxCal4.2 modelled weighed mean ages for the

303 respective age-depth assignments (Table 4). Parts of the uppermost and/or

304 lowermost layers in some profiles do not overlap with the length of core #5. The

305 chronology for these parts had therefore to be estimated using the modelled

306 sedimentation rate of the respective lithostratigraphic units (Fig. 3B, Table 4).

307 The new composite age model for core #5 (Muschitiello *et al.* 2015b) compares

308 well with the previous age model (Steinthorsdottir *et al.* 2013, 2014) in terms of

309 shape of the age-depth relationship and age output values. It however provides a

310 higher number of time constraints, especially between 13 and 11 cal. ka BP

311 (Muschitiello *et al.* 2015b).

312   When plotted on the new time scale of core #5, the main features of the

313 six LOI/TOC curves fall within the same time interval, such as the decrease in

314 LOI/TOC values at 13 cal. ka BP, their peak between 12.8 and 12.7 cal. ka BP, as

315 well as the mid-point of their gradual rise at 11.5 cal. ka BP (Fig. 3B). Moreover,

316 modelled ages differ by less than 150 years for both the 'Borrobol' and Askja-S

317 tephra and by less than 50 years for the Hässeldala tephra between cores #1 and

318 3 (Fig. 3B). The good temporal correspondence of the main features in the six

319 sediment cores gives confidence in the statistical curve alignments and provides

320 a new chronological basis for discussing the Lateglacial environmental and

321 climatic history of southern Sweden.

322

323 Local and regional environmental and climatic development

324 *>14.1 cal. ka BP*

325 Glacial varve chronologies, glacial stratigraphy and geomorphology, and pollen

326 stratigraphic studies in Blekinge province, southernmost Sweden, reconstruct a

327 rapid decay of the Scandinavian Ice Sheet margin in response to the temperature

328   rise at the start of the Bølling-Allerød interstadial at 14.7 cal. ka BP (Björck &

329   Möller 1987; Ringberg 1991; Wohlfarth *et al.* 1994; Lundqvist & Wohlfarth 2001;

330   Anjar *et al.* 2013). The combination of ice sheet load, ice sheet melt and isostasy

331   created a large ice lake in the Baltic Sea basin (Björck 1995; Andrén *et al.* 2011),

332   whose highest shoreline reached up to ~65-67 m a.s.l. in Blekinge (Björck 1981;

333   Ringberg 1991).

334   The local glacial varve chronology shows that coastal areas in southern

335   Blekinge had become free of active ice within 100 years (Fig. 5A) and that the

336   formation of the highest coastline at 65-67 m a.s.l. likely corresponds to an ice

337   marginal position at around local varve year 0 (Ringberg 1991). Rapid land uplift

338   followed coastal deglaciation and led to an apparent lowering of the Baltic Ice

339   Lake shoreline (Björck 1981; Wohlfarth *et al.* 1994). The deposition of

340   exceptionally thick varves, which can be seen in many clay-varve diagrams from

341   Blekinge (corresponding to local varve years +88 to +220) (Ringberg 1991;

342   Wohlfarth *et al.* 1994), signals accelerated ice sheet melt and likely correlates to

343   fluvio-glacial delta surfaces at around 55 m a.s.l. (Björck 1981). More or less

344   coinciding with the appearance of the thick varves, the area around Hässeldala

345   Port became free of active ice, as seen in the deglaciation ages for sites such as

346   Trehörnan, Hemsjön, Kroksjön II and Skälgylet (Fig. 5B, Table 5). Glacial varves

347   did however not form at Hässeldala Port since the site was located at much

348   shallower depths and close to the shoreline of the Baltic Ice Lake (Fig. 5C). Pollen

349   stratigraphic studies of the varved-clay succession of Farslycke (Ising, 1998) and

350   Kroksjön II (Björck 1981) (Fig. 5B) and plant macrofossil finds of *Salix polaris*, *S.*

351   *reticulata*, *S. herbacea*, *Dryas octopetala*, and *Betula nana* in the thick varves

352   (Wohlfarth *et al.* 1994) suggest that herb and shrub vegetation had become

353   established on ice-free land areas. Pollen assemblages (Farslycke, Kroksjön) and

354   [14]C ages on terrestrial plant remains (Farslycke, Skälgylet) assign the thick

355   varves to the Bølling pollen zone (Björck 1981, 1984; Björck & Möller 1987; Ising

356   1998; Wohlfarth & Possnert 2000; Lundqvist & Wohlfarth 2001). Varves

357   assigned to local varve years +220 to +360 become gradually thinner displaying

358   a greater distance to the rapidly melting ice sheet margin, which was now

359   located some 50-100 km to the north of Blekinge's present coastline, and drained

360   by large overland rivers (Björck & Möller 1987; Möller 1987). Lake isolation

361   studies, combined with pollen stratigraphies, show that land uplift was still rapid

362   and that the shoreline of the Baltic Ice Lake was successively lowered to around

363   50-55 m a.s.l. at the end of the regional Bølling pollen zone (Figs 5B, C) and to

364   around 45-50 m a.s.l. (Fig. 5D) at the end of the regional Older Dryas pollen zone

365   (Björck 1981, 1984).

366   The gradual emergence of new land areas meant that Hässeldala Port's

367   location changed from an archipelago setting during the Bølling pollen zone to

368   further inland during the Older Dryas pollen zone (Figs 5C, D). The bottommost

369   silty fine sand (unit 1) in Hässeldala Port's successions (Figs 2, 6A) could derive

370   from melting of stagnant ice or run-off from poorly vegetated slopes. Coleoptera

371   assemblages suggest mild and cool summers during this early period with mean

372   summer air temperatures of about 14 °C (Watson 2008) and the presence of

373   *Hippophaë rhamnoides* and *Nymphaea alba* in the aquatic pollen record of

374   Hässeldala Port (Andersson 2004) indicates minimum mean July temperatures

375   of >10 °C and possibly as much as 11-12 °C (Iversen, 1954; Kolstrup 1980). In

376   contrast, mean July surface water temperatures reconstructed from chironomid

377   assemblages are around 7-8 °C (Fig. 6E) and may represent a lake water

378   temperature that was strongly influenced by run-off from stagnant ice. The herb,

379   grass, shrub and dwarf-shrub dominated pollen assemblages (HÄP-1)

380   (Andersson 2004; Wohlfarth *et al.* 2006) suggest that these lowermost

381   sediments were deposited during the regional Older Dryas pollen zone (Figs 6H,

382   J).

383   Plant macrofossil finds and pollen stratigraphic records in Blekinge

384   dating to the regional Older Dryas pollen zone (Berglund 1966; Björck 1981;

385   Wohlfarth *et al.* 1994, 2006) reveal a shrub-grass-herb vegetation, that

386   comprised *Artemisia, Betula nana*, *Calluna vulgaris*, *Caltha palustris*, *Dryas

387   octopetala*, *Empetrum nigrum*, *Ephedra*, *Helianthemum*, *Hippophaë rhamnoides*,

388   *Juniperus communis*, *Plantago*, *Polygonum*, *Rumex*, *Saxifraga*, *Salix polaris*, and

389   *Urtica* (Table 6). Pollen of *Populus tremula* (Berglund 1966) and plant

390   macrofossil finds of *Betula pubescens* (Wohlfarth *et al.* 1994) (Table 6) moreover

391   point to the regional presence of shrub-like trees. Regional minimum mean July

392   temperatures of >10 °C for *Betula pubescens* (Iversen 1954) compare well to

393   those inferred from Coleoptera species and pollen in Hässeldala's sediments.

394

395 *14.1 – 12.7 cal. ka BP*

396 Hässeldala's silty clay, gyttja clay and clayey gyttja (units 2 – 7) and the

397 accompanying LOI curve demonstrate a gradually higher organic matter content

398 of the sediments, but also that minerogenic inputs still dominate (Figs 6A, B). LOI

399 displays a first marked increase at 13.7 cal ka BP, coinciding with the start of unit

400 3, and thereafter fluctuates between lower (13.5-13.4 cal. ka BP; 13.05-12.95 cal.

401 ka BP) and higher values (13.7-13.55 cal. ka BP; 13.3-13.1 cal. ka BP; 12.9-12.7

402 cal. ka BP) (Fig. 6B). Accumulation rates seem to have been rather stable

403 throughout this time interval, except for around 14.1-13.7 and 13.0-12.9 cal. ka

404 BP, when sediment accumulation was slightly higher (Kylander *et al.* 2013).

405   The tephra layer that had been assigned to the Borrobol tephra (Davies *et*

406 *al.* 2003, 2004; Wohlfarth *et al.* 2006) (Fig. 6F), but has been discussed as being

407 an equivalent of the Penifiler tephra (Mathews *et al.* 2011) falls within the

408 interval of low LOI values. The core-to-core alignment and the new chronology

409 for core #5 suggest that this tephra layer dates to around 14.1-13.7 cal. ka BP.

410   In conjunction with the increase in LOI values at 13.7 cal. ka BP (Fig. 6B),

411 diatom-inferred lake water pH shifts to more acid values (Fig. 6C). This distinct

412 shift could be the result of increased surface flow that transported organic acids

413 from surrounding soils into the shallow lake (Ampel *et al.* 2014) and could

414 indicate that the catchment vegetation had become denser. Lake waters become

415 neutral around 13.5 cal. ka BP and remain, apart from a few minor fluctuations,

416 around a pH of 7 until 12.7 cal. ka BP (Fig. 6C). The diatom assemblages and the

417 crysophyte:diatom ratios (C:D) in the lowermost diatom zone (DAZ-I; 14.1-13.2

418 cal. ka BP) (Fig. 6C) suggest cold lake water conditions, low light and nutrient

419 availability, but also a gradual shortening of the ice-covered season (Ampel *et al.*

420 2014). Leaf-wax derived hydrogen isotopes, $\delta D_{n}\text{-}C_{21}$ and $\Delta\delta D_{terr\text{-}aq}$, which reflect

421 the isotopic composition of the source moisture and terrestrial evaporation,

422 respectively indicate a saline moisture source and minor shifts between drier

423 and wetter conditions (Fig. 6D). However the measurement errors are too large

424 to render these values significant. Chironomid-derived mean July surface water

425 temperatures show a step-wise increase from 8 °C at 14.1 cal. ka BP to maximum

426 values of 12-13 °C at 13.2-13.1 cal. ka BP (Fig. 6E). Coleoptera assemblages are

427 still composed of species typical of cool and mild climates, but reconstructed

428 summer temperatures now reach >14 °C (Watson 2008) and seem to be

429 comparable to chironomid-inferred temperatures.

430   The Hässeldala Port proxies suggest marked changes between 13.2 and

431 12.7 cal. ka BP. In diatom zone DAZ-II (13.2-12.6 cal. ka BP) (Fig. 6C) the habitat

432 structure in the shallow lake changes, open water taxa decline, but the diatom

433 flora becomes more diverse and attached-growing species become more

434 abundant. This points to denser aquatic vegetation, possibly in response to a lake

435 level lowering and/or higher nutrient availability (Ampel *et al.* 2014). The C:D

436 ratio shows a decline in the number of crysophyte cysts relative to diatoms,

437 which points to a shorter ice-covered season (Fig. 6C). $\delta D_{n\text{-}C_{21}}$ values start to

438 decrease at 13.2 cal. ka BP and reach minimum values between 13.0-12.8 cal. ka

439 BP, coincident with higher $\Delta\delta D_{terr\text{-}aq}$ values (Fig. 6G). This shift in hydrogen

440 isotope values suggests a freshening of the marine moisture source region and

441 distinctly drier conditions at Hässeldala Port (Muschitiello *et al.* 2015b). The

442 trend of decreasing $\delta D_{n\text{-}C_{21}}$ values and increasing $\Delta\delta D_{terr\text{-}aq}$ values was shortly

443 interrupted at 12.7 cal. ka BP, when more saline moisture reached the site and

444 conditions became wetter. The observed two-step decrease in δD_{aq} values (13.0-

445 12.8 and after 12.7 cal. ka BP) has been interpreted as a progressive freshening

446 of the Atlantic precipitation water source for Hässeldala Port caused by the

447 melting of the Fennoscandian Ice Sheet (Muschitiello *et al.* 2015b). The distinct

448 shift in hydrogen isotope values and diatom assemblages around 13.2 cal. ka BP

449 coincides with a decline in mean July surface water temperatures to around 10-

450 11 °C (Fig. 6C-E).

451   The main features in local pollen assemblage zones HÄP-2 (14.1-13.2 cal.

452 ka BP) (rise in *Juniperus communis* pollen percentages) and HÄP-3 (13.2-12.7 cal.

453 ka BP) (increase in *Empetrum* and Ericales pollen values) (Andersson 2004;

454 Wohlfarth *et al.* 2006) allow for a correlation to the regional Allerød I and II

455 pollen zones (Björck & Möller 1987), respectively (Fig. 6H, J). *Nymphaea alba*

456 pollen are continuously present in low numbers in HÄP-2 and HÄP-3 (Andersson

457 2004) and thus suggest that minimum mean July temperatures were >10 °C

458 (Kolstrup 1980). HÄP-3 correlates to local pollen zone Hä-1 and to parts of local

459   pollen zone Hä-2, which were recently established on core #6 (Karlatou-

460   Charampopoulou 2016) (Fig. 6I) and detail the vegetation changes that occurred

461   at the regional Allerød/Younger Dryas transition (see below).

462   Pollen stratigraphic data sets for Blekinge (Berglund 1966; Björck &

463   Möller 1987) show that herbs and shrubs still dominate, but that the regional

464   vegetation had become more diverse. Plant species now also include *Astralagus*

465   *alpinus, Cerstium alpinum, Dryopteris, Isoëtes, Jasione montana, Lycopodium,*

466   *Lastrea, Myriophyllum alterniflorum, Populus tremula, Potentilla palustris, Prunus*

467   *padus, Pimpinella, Polypodium, Ranunculus, Rubus, Sanguisorba, Sorbus, Typha*

468   *latifolia* and *Valeriana officinalis* (Berglund 1966) (Table 6). Moreover, plant

469   macro-remains of *Betula pubescens* have been reported (Berglund 1966).

470   Minimum mean summer temperatures based on indicator species, such as

471   *Betula pubescens* (Iversen 1954), *Hippophaë rhamnoides, Typha latifolia*

472   (Kolstrup 1980), and *Jasione montana* (Kolstrup 1979) (Table 6), suggest that

473   minimum mean July temperatures were around 12-15 °C. However these values

474   relate to the whole of the regional Allerød pollen zone and do not allow any

475   differentiation of changes through time. The chironomid-based summer surface

476   water temperature reconstruction and the age model for Hässeldala Port now

477   provide a more detailed view of the temperature evolution between 14.1 and

478   12.7 cal. ka BP and indicate that warm mean July temperatures were only

479   attained between 13.4-13.1 cal. ka BP (Fig. 6E).

480   The increase in organic matter content seen in Hässeldala Port's

481   sediments between 12.9-12.7 cal. ka BP (Figs 3A, 6B) is a feature that is typical

482   for many Lateglacial sequences in southern Sweden (Björck & Möller 1987;

483   Berglund *et al.* 1994). It has been long argued that this increase represents the

484   in-wash of topsoil material that was released during the final melting of remnant

485   ice or could indicate a lake level lowering due to drier climatic conditions

486   (Digerfeldt 1971). A C/N ratio of 13 and bulk $\delta^{13}C$ values of around -18‰ for

487   Hässeldala Port do not support increased in-wash of terrestrial organic material,

488   but rather point to a dominance of aquatic sourced organic matter (Kylander *et*

489   *al.* 2013). Moreover, higher $\Delta\delta D_{terr-aq}$ values and lower mean July temperatures

490   that coincide with the peak in LOI indicate drier and slightly colder conditions

491   (Figs 6D, E), which could have led to a lake level lowering. This scenario

492 compares well with the findings of Ampel *et al.* (2014), who had suggested a

493 lowering of the lake level as a result of drier conditions. A lower lake level and

494 expansion of the aquatic vegetation could have raised the nutrient level in the

495 already shallow lake as reflected by high LOI values.

496

497 *12.7-11.8 cal. ka BP*

498 The lithological boundary between the dark brown clayey gyttja (unit 7) and the

499 greenish-brown/brown clayey gyttja (unit 8) is reflected by a decrease in LOI

500 values (Figs 6A, B). LOI values remain low until *c.* 11.8 cal. ka BP and gradually

501 increase thereafter (Fig. 6B). This increase is coupled to a change in sediment

502 colour and lithology (unit 9). The initial decrease and later increase in lake

503 organic productivity is mirrored by geochemical proxies (Kylander *et al.* 2013),

504 which suggest relatively stable conditions between 12.7 and 12.0 cal. ka BP, but

505 changes in source material and/or hydrology and in aquatic productivity

506 thereafter.

507 Opportunistic diatom taxa (e.g. *Staurosirella pinnata*), which compete

508 well under challenging environmental conditions, increase in abundance in

509 diatom zone DAZ-III (12.6-11.8 cal. ka BP), as do the relative numbers of

510 chrysophyte cysts (12.6-12.3 cal. ka BP) (Ampel *et al.* 2014) (Fig. 6C). The

511 increase in crysophyte cysts suggests that nutrient levels had decreased, which

512 would be in line with lower lake organic productivity as inferred by lower LOI

513 values (Fig. 6B). This change in lake status (low nutrient, low productivity)

514 together with colder temperatures and longer ice-cover seasons gave certain

515 diatom species an advantage (Ampel *et al.* 2014).

516 The decline in mean July surface water temperatures, which starts at 12.7

517 cal. ka BP, continues until 12.5-12.4 cal. ka BP, when the lowest reconstructed

518 temperatures of 8 °C are reached (Fig. 6E). Coincident with the decline in

519 temperatures, $\delta D_{n\text{-}C_{21}}$ values decrease and $\Delta\delta D_{terr\text{-}aq}$ values increase, suggesting a

520 fresher moisture source and progressively drier conditions (Fig. 6D). Mean July

521 surface water temperatures fluctuate and stay around 9-10 °C between 12.4-11.9

522 cal. ka BP, but subsequently start rising again from 9 °C to 12 °C (Fig. 6E). This

523 steady rise more or less coincides with distinct changes in $\delta D_{n\text{-}C_{21}}$ and $\Delta\delta D_{terr\text{-}aq}$

524 values (Fig. 6D), which show a shift towards a more saline marine moisture
525 source of precipitation and wetter conditions around 11.8 cal. ka BP
526 (Muschitiello *et al.* 2015b).

527 The decrease in *Empetrum* pollen values and the increase in herb and
528 grass pollen percentages, especially for *Artemisia*, defines local pollen zone HÄP-
529 4 (Andersson 2004; Wohlfarth *et al.* 2006) (12.7-11.7 cal. ka BP). This local
530 pollen zone, which partly overlaps with local pollen zones Hä-3, Hä-4 and Hä-5
531 on core #6 (Karlatou-Charalampopoulou 2016), was correlated to the regional
532 Younger Dryas pollen zone (Figs 6H-J) of Berglund (1966) and Björck & Möller
533 (1987) (Andersson 2004; Wohlfarth *et al.* 2006) (see below). *Nymphaea alba*
534 pollen, which are present during HÄP-4 (Andersson 2004) suggest minimum
535 mean July temperatures of >10 °C (Kolstrup 1980), which compares to those
536 reconstructed from chironomid assemblages (Fig. 6E).

537 Pollen stratigraphies for Blekinge (Berglund 1966; Björck & Möller 1987)
538 show that the expanding herb and shrub vegetation comprised *Artemisia,*
539 *Astralagus alpinus, Betula nana, Calluna vulgaris, Cerastium alpinum,*
540 *Chamaenerion alpinum, Dryas octopetala, Dryopteris, Empetrum nigrum, Ephedra,*
541 *Helianthemum, Hippophaë, Jasione montana, Juniperus communis, Lycopus*
542 *europaeus, Minuartia, Myriophyllum alterniflorum, M. spicatum, M. verticillatum,*
543 *Oxytropis capestris, Oxyria digyna, Plantago, Polygonum, Potentilla palustris,*
544 *Populus tremula, Ranunculus, Rumex acetosella, Rubus, Sanguisorba, Sorbus,*
545 *Saxifraga, Selaginella selaginoides,* and *Urtica* (Table 6). Interestingly, also *Pinus*
546 *sylvestris* macrofossil remains have been reported for this time interval
547 (Berglund 1966). This is surprising given that these had not been found during
548 the Allerød pollen zone. On the other hand, especially high pollen values for
549 *Pinus* in Allerød lake sediments in Blekinge could be an indication for the
550 presence of these trees prior to the regional Younger Dryas pollen zone (Björck
551 1979). *Pinus* may have thus survived in micro-climatically favourable habitats or
552 the macrofossil finds of *Pinus sylvestris* relate to the very end of the regional
553 Younger Dryas pollen zone.

554 Plant indicator species (Table 6), such as *Hippophaë rhamnoides,*
555 *Myriophyllum alterniflorum, M. spicatum, M. verticillatum* and *Jasione montana,*
556 would suggest that minimum mean summer temperatures reached 10-12 °C

557   (Kolstrup 1979; 1980). These values however relate to the regional Younger

558   Dryas pollen zone in general and do not allow differentiation of changes through

559   time. The chironomid-based temperature reconstruction for Hässeldala Port

560   shows that mean July surface water temperatures fluctuated between 8-10 °C

561   during the Younger Dryas and rose to >10 °C only at 11.9 cal. ka BP (Fig. 6E).

562   Since *Pinus sylvestris* requires minimum mean summer temperatures of >12 °C

563   (Iversen 1954), we speculate that the macrofossil finds reported by Berglund

564   (1966) stem from the latest part of the regional Younger Dryas pollen zone,

565   when summer temperatures had already increased.

566

567   *In and out of the Younger Dryas pollen zone*

568   It is interesting to look closer into the sequence of events around the start and

569   end of the regional Younger Dryas pollen zone since several of Hässeldala Port's

570   proxies (LOI, hydrogen isotopes and diatom assemblages) have been analysed on

571   the same split samples of core #5. The chironomid-derived temperature

572   reconstruction and the pollen stratigraphies were however established on

573   parallel cores that were aligned to the chronology of core #5 using the approach

574   of Muschitiello *et al.* (2015b). The former therefore allow for a direct

575   comparison, independent of the age assignment, while minor time lags detected

576   for the latter could be an artefact because age model errors are not taken into

577   account here.

578   The most recent pollen stratigraphy for Hässeldala defines local pollen

579   zone Hä-2 (12.77-12.54 cal. ka BP) as a transition zone between the regional

580   Allerød and Younger Dryas pollen zones (Figs 6I, J) (Karlatou-Charalampopoulou

581   2016). This pollen zone is characterised by a first increase in *Artemisia* pollen

582   values and a decrease in pollen concentrations. These changes seem to have

583   occurred more or less coincident with several other proxies. Sediment organic

584   matter content declines, the number of crystophyte cysts over diatoms starts to

585   increase (Fig. 6C), hydrogen isotope proxies show a brief return to wetter

586   conditions at *c.* 12.7 cal. ka BP that was followed by progressively drier

587   conditions (Fig. 6D) and chironomid-inferred summer surface lake water

588   temperatures decline (Fig. 6E). Slight differences between the lower boundaries

589 of HÄP-4 and Hä-3 are due to how pollen zones transitions were originally

590 defined, as the increase in *Artemisia* pollen values in core #3, which is

591 comparable to the lower boundary of Hä-3, actually already occurs at 12.7 cal. ka

592 BP (Andersson 2004).

593   Hä-5 (11.85-11.58 cal. ka BP) reflects the transition zone between the

594 regional Younger Dryas and Preboral pollen zones (Figs 6I, J) and is defined by

595 decreasing *Juniperus* and *Artemisia* pollen percentages and rising *Empetrum*

596 pollen values (Karlatou-Charalampopoulou 2016). The start of Hä-5 predates the

597 transition between pollen zones HÄP-4 and HÄP-5 (11.7 cal. ka BP), but

598 coincides with rising sediment organic matter content, changes in diatom

599 assemblages, marked shifts in hydrogen isotope values and a rise in chironomid-

600 inferred summer surface water temperatures (Fig. 6B-I).

601   Hässeldala Port's proxies thus provide no clear evidence for distinct local

602 lags in response to regional climatic changes at the start and end of the Younger

603 Dryas. Minor divergences, as seen in the comparison between the two pollen

604 stratigraphic records (Fig. 6H, I), are an artefact of where and how pollen zone

605 boundaries are drawn and defined.

606

607 *11.8-10 cal. ka BP*

608 Hässeldala Port's sediments shift from clayey gyttja (unit 8) to gyttja (units 9-11)

609 around 11.8 cal. ka BP and to peaty gyttja (unit 12) at 10.9 cal. ka BP (Fig. 6A).

610 The steady increase in LOI values and subsequent values of >80% depict the

611 increase in sediment organic matter and show that the small lake gradually filled

612 in (Fig. 6B). This is also reflected in the diatom assemblages of DAZ-IV, which

613 suggest a transition towards a less alkaline mire environment that gradually

614 turned into a rather dry mire environment (Ampel *et al.* 2014). Coleoptera,

615 which are typical of acid bog environments and dry shrub heathland, such as

616 *Amara alpina* and *Olophrum boreale* now appear (Watson 2008). The trend to

617 overall wetter conditions as seen in decreasing $\Delta\delta D_{terr-aq}$ values was briefly

618 interrupted around 11.5 cal. ka BP, when hydrogen isotope values suggest both a

619 freshening of the marine sources of precipitation and a return to slightly drier

620 conditions (Fig. 6D). The timing of this shift compares to the Preboreal

621   Oscillation, a short cooling phase identified in North Atlantic paleo-records
622   (Björck *et al.* 1996, 1997) and predates the oscillation discussed earlier by
623   Wohlfarth *et al.* (2006) based on the LOI curve of core #3. The Hässeldala tephra,
624   identified in core #1 and 3 (Davies *et al.* 2003, 2004; Wohlfarth *et al.* 2006),
625   occurs around 11.3 cal. ka BP and thus after the oscillation seen in the hydrogen
626   isotope proxies (Fig. 6D, F). Cryptotephra, which has been geochemically
627   assigned to the Askja-S tephra was also found in cores #1 and 3 and can now be
628   dated to around 10.9-10.7 cal. ka BP (Fig. 6F).

629   Local pollen zone HÄP-5 (11.7-11.3 cal. ka BP) (Andersson 2006)
630   overlaps with local pollen zones Hä-5 and Hä-6 in core #6 (11.85-11.3 cal. ka BP)
631   (Karlatou-Charalampopoulou 2016) (Fig. 6H, I). The distinct peak in *Empetrum*
632   pollen percentages, a decrease in *Artemisia* pollen values and overall a slight
633   increase in tree pollen, mainly of *Betula*, allows correlations to the YD-PB
634   transition zone of Berglund (1966) and Björck & Möller (1987). The YD-PB
635   transition zone has been assigned to the early part of the regional Preboreal
636   pollen zone (Björck *et al.* 1996), thus marking the start of the Holocene.
637   Macroscopic charcoal appears in large quantities around 11.8-11.6 cal. ka BP and
638   the first macroscopic finds of *Betula pubescens* occur at 11.6-11.4 cal. ka BP
639   (Wohlfarth *et al.* 2006) (Fig. 6G). Tree pollen percentages increase further in
640   HÄP-6 (11.3-10.9 cal. ka BP) and HÄP-7 (10.9-10.3 cal. ka BP), herb and shrub
641   pollen decline (Andersson 2006), and the presence of *Pinus sylvestris* is attested
642   by finds of needles at 11.0 cal. ka BP (Wohlfarth *et al.* 2006) (Fig. 6G, H). Aquatic
643   pollen of *Typha angustifolia* and *Nymphaea alba* in HÄP-6 and of *Myriophyllum*
644   *alterniflorum/spicatum* in HÄP-7 (Andersson 2004) suggest that minimum July
645   temperatures had increased distinctly and may have reached >14 °C (Kolstrup
646   1980). Wetter conditions, as suggested by decreasing $\Delta\delta D_{terr-aq}$ values (Fig. 6D),
647   and warmer summers likely favoured the further establishment and expansion
648   of trees in Hässeldala Port's catchment. HÄP-6 and HÄP-7 are correlated to the
649   regional Preboreal pollen zones of Berglund (1966).

650   The vegetation during the regional early Preboreal pollen zone in
651   Blekinge now also included *Botumus umbellatus*, *Caltha palustris, Isoëtes*
652   *lacustris, Littorella uniflora, Menyanthes trifoliata, Rubus fruticosus,* and *Typha*
653   *latifolia,* and *Pinus sylvestris* (Berglund, 1966) (Table 6). This latter species, as

654   well as the presence of *Typha latifolia* and *Betula pubescens*, in addition to other

655   indicator species, suggests that minimum mean July temperatures now reached

656   >12 °C (Iversen 1954; Kolstrup 1980). This assumption compares nicely to

657   higher summer temperatures inferred from chironomid assemblages (Fig. 6E)

658   and aquatic pollen.

659

660   Wider implications

661

662   Hässeldala Port's pollen-stratigraphic records of cores #3 (Andersson 2004;

663   Wohlfarth *et al.* 2006) and #6 (Karlatou-Charampopoulou 2016) and the refined

664   age model now provide a new chronological template for Lateglacial climatic and

665   environmental changes in southern Sweden (Table 7). Andersson's (2004) HÄP-

666   1, which is correlated to the regional Older Dryas pollen zone, is dated to >14.06

667   cal. ka BP. HÄP-2 compares to the regional Allerød I pollen zone and ranges

668   between 14.06 and 13.24 cal. ka BP and HÄP-3 or the regional Allerød II pollen

669   zone dates to between 13.24 and 12.67 cal. ka BP. Wohlfarth *et al.* (2006) had

670   earlier correlated local pollen zone HÄP-4 (12.67-11.68 cal. ka BP) with the

671   regional Younger Dryas pollen zone, but this correlation now needs to be

672   revised, following the high-resolution pollen stratigraphy of core #6 (Karlatou-

673   Charampopoulou 2016). This latter work shows that a Late Allerød/early

674   Younger Dryas transition zone (Hä-2: 12.77-12.54 cal. ka BP) overlaps with parts

675   of Andersson's (2004) pollen zones HÄP-3 and HÄP-4 (Fig. 6I, J) and suggests

676   that changes in vegetation composition already commenced at 12.77 cal. ka BP

677   (Table 7). Karlatou-Charampopoulou's (2016) local pollen zones Hä-3 and Hä-4

678   correlate to the regional Younger Dryas pollen zone as defined by Björck &

679   Möller (1987) and extend between 12.54 and 11.85 cal. ka BP (Table 7). The

680   transition between the regional Younger Dryas and Preboreal pollen zones

681   (Berglund 1966; Björck & Möller 1987), which Björck *et al.* (1996) had assigned

682   to the early Holocene, is also clearly seen in Hässeldala Port's pollen

683   stratigraphy. It is represented by pollen zone Hä-5 (Karlatou-Charampopoulou

684   2016) (Fig. 6 I, J) and dated to 11.85-11.58 cal. ka BP (Table 7).

685   Muschitiello & Wohlfarth (2015) earlier discussed the time-transgressive

686 nature of vegetation changes in northern Europe around the Allerød – Younger

687 Dryas transition using well-dated pollen stratigraphic records. They showed that

688 the early response seen in Sluggan Bog, Northern Ireland (Walker *et al.* 2012)

689 (13.0 cal. ka BP) predates vegetation shifts in sites located further to the east by

690 *c.* 300-350 years (Fig. 7) and hypothesize that this may have been caused by

691 regional cooling around the Nordic Seas. Hässeldala Port now adds an important

692 data point to this network and supports Muschitiello & Wohlfarth's (2015)

693 conclusions that vegetation shifts reconstructed for sites in Norway, Sweden and

694 western Germany postdate those in Northern Ireland and also occurred 100-250

695 years later than the onset of Greenland Stadial 1 (Fig. 7). The change in

696 vegetation composition seen in Kråkenes (Norway) at 12.75-12.7 cal. ka BP

697 (Birks *et al.* 2000), Madtjärn (Swedish west coast) at 12.7-12.6 cal. ka BP (Björck

698 *et al.* 1996), Hässeldala Port between 12.77-12.54 cal. ka BP and in Meerfelder

699 Maar (Germany) at 12.7-12.65 cal. ka BP (Rach *et al.* 2014) thus only took place

700 at a time when critical threshold temperatures had been reached and when

701 Greenland ice cores reflect the establishment of full stadial climate conditions

702 and a stadial atmospheric circulation regime (Steffensen *et al.* 2008; Rach *et al.*

703 2014; Muschitiello & Wohlfarth 2015).

704   This hypothesis can be tested by comparing the timing of hydroclimate

705 shifts and vegetation records using the two available detailed δD stratigraphies

706 of Hässeldala Port (Muschitiello *et al.* 2015b) and Meerfelder Maar (Rach *et al.*

707 2014). The δD_{aq} records from Hässeldala Port and Meerfelder Maar show a

708 consistent trend towards more negative values at the start of the Younger Dryas

709 pollen zone (Fig. 8). This suggests large-scale cooling and more negative δD

710 values of the marine moisture source of precipitation – the North Atlantic Ocean

711 – associated with a southward diversion of the storm track trajectories and sea-

712 ice expansion (Rach *et al.* 2014). More interestingly, the two records display an

713 opposite hydro-climate behaviour between southern Sweden and western

714 Germany during the Late Allerød pollen zone/Greenland Interstadial 1a (*c.* 13.1-

715 12.9 cal. ka BP), with relatively lower δD_{aq} values at Hässeldala Port and

716 relatively higher δD_{aq} values at Meerfelder Maar. This pattern is also evident in

717 the $\Delta\delta D_{terr-aq}$ profiles, which suggest drier conditions at Hässeldala Port as

22

718 opposed to more humid conditions at Meerfelder Maar (Fig. 8). Muschitiello *et al.*

719 (2015b) suggested that such opposite hydro-climate patterns prior to the start of

720 the Younger Dryas are an expression of increased freshwater forcing from the

721 Fennoscandian Ice Sheet to the Nordic Seas, which affected the hydro-climate

722 system at synoptic scale. Climate model simulations indeed show that freshwater

723 forcing from the Fennoscandian Ice Sheet results in relatively lower atmospheric

724 pressure over the western sector of Europe and Greenland, whereas Northern

725 Europe is affected by relatively higher-pressure conditions (Muschitiello *et al.*

726 2015b). This scenario could explain the spatially complex differences in moisture

727 availability across the North Atlantic (Muschitiello *et al.* 2015b). The hydro-

728 climate records from Hässeldala Port and Meerfelder Maar also show that

729 southern Sweden likely experienced drier conditions as compared to Western

730 Europe during the Younger Dryas (Fig. 8). This is in line with evidence of

731 increasing continentality and more severe aridity in Europe from south to north

732 (e.g. Birks *et al.* 2014).

733   The transition out of the Younger Dryas is equally interesting. At *c.* 11.9

734 cal. ka BP, δD_{aq} values from Hässeldala Port and Meerfelder Maar start to rise

735 and increase by $\sim$40‰ and 30‰, respectively (Fig. 8). The shifts in δD_{aq} are

736 paralleled by changes in $\Delta\delta D_{terr-aq}$, which indicate progressively wetter

737 conditions both in Western Germany and southern Sweden (Fig. 8). Moreover,

738 these hydro-climate shifts were initiated *c.* 300 years earlier in Europe than the

739 transition into the Holocene in Greenland (Fig. 8). This sequence of events is in

740 agreement with the hypothesis of a gradual northward recession of the North

741 Atlantic sea-ice margin during the second half of the Younger Dryas, which paved

742 the way for a strengthening of the Atlantic Meridional Overturning Circulation

743 associated with the start of the warm Holocene interglacial (e.g. Lane *et al.* 2013;

744 Pearce *et al.* 2013; Bartolomé *et al.* 2015).

745   Concluding, we find distinct and in-phase gradual perturbations of the

746 hydro-climate system across the North Atlantic leading the transitions into the

747 Younger Dryas stadial and the Holocene interglacial. These features imply that

748 complex atmosphere-ocean feedbacks are at work prior to an abrupt climate

749 change.

750

751

Conclusions

753

754   The Lateglacial sedimentary successions from the ancient lake at Hässeldala Port

755   in southern Sweden spans the period 14.5-9.5 cal. ka BP and forms one of the

756   best chronologically-constrained sites in Europe. Hässeldala Port's sediments

757   were analysed using a variety of proxies that allow capturing local and regional

758   climatic and environmental signals. The refined age model for the multi-proxy

759   records (lithology, geochemistry, pollen, diatoms, chironomids, biomarkers,

760   hydrogen isotopes) now enables discussing environmental and climatic changes

761   in a regional context and provides a new chronological framework for the

762   vegetation development in southern Sweden. Hässeldala Port's multi proxy

763   records imply that regional cooling and hydroclimate changes in the Nordic Sea

764   region led to more or less synchronous local responses in and around the ancient

765   lake. These changes were however offset by several hundred years as compared

766   to the start and end of Greenland stadial GS-1. Hässeldala thus provides further

767   insights into the spatial and temporal complexity of environmental and

768   hydroclimatic responses to North Atlantic rapid climate shifts.

769

770

771   References

772

773   Ammann, B., van Raden, U. J., Schwander, J., Eicher, U., Gill, A., Bernasconi, S. M.,
774   van Leeuwen, J. F. N., Lischke, H., Brooks, S. J., Heiri, O., Nováková, K., van
775   Haardenbroek, M., von Grafenstein, U., Belmecheri, S., van der Knaap, W.
776   O., Magny, M., Eugster, W., Colombaroli, D., Nielsen, E., Tinner, W. &
777   Wright, H. E. 2013: Responses to rapid warming at Termination 1a at
778   Gerzensee (Central Europe): Primary succession, albedo, soils, lake
779   development, and ecological interactions. *Palaeogeography,*
780   *Palaeoclimatology, Palaeoecology 391*, 111-131.
781   Ampel, L., Kylander, M. E., Steinthorsdottir, M. & Wohlfarth, B. 2014: Abrupt
782   climate change and early lake development – the Lateglacial diatom flora
783   at Hässeldala Port, southeastern Sweden. *Boreas 44*, 94-102.
784   Andersson, M. 2004: *Pollenstratigraphic response for tephra horizons during the*
785   *last glacial – interglacial transition (LGIT) in southernmost Sweden*. M. Sc.
786   thesis 4108, Stockholm University, 65 pp.

787 Andrén, T., Björck, S., Andrén, E., Conley, C., Zillén, L. & Ajar, J. 2011: The
788   development of the Baltic Sea Basin during the last 130 ka. *In* Harff, J.,
789   Björck, S. & Hoth, P. (eds.): *The Baltic Sea Basin*, 75-97. Springer Verlag,
790   Berlin/Heidelberg.
791 Anjar, J., Larsen, N. K., Håkansson, L., Möller, P., Linge, H., Fabek, D. & Xu, S. 2013:
792   A [10]Be-based reconstruction of the last deglaciation in southern Sweden.
793   *Boreas 43*, 132-148.
794 Bartolomé, M., Morenao, A., Sancho, C., Stoll, H. M., Cacho, I., Spötl, C., Belmonte,
795   A., Edwards, R. L., Cheng, H. & Hellstrom, J. C. 2015: Hydrological change
796   in Southern Europe responding to increasing North Atlantic overturning
797   during Greenland Stadial 1. *Proceedings of the National Academy of*
798   *Sciences 112*, 6568–6572.
799 Berglund, B. E. 1966: Late-Quaternary vegetation in eastern Blekinge, south-
800   eastern Sweden. *Opera Botanica 12*, 5-180.
801 Berglund, B. E., Bergsten, H., Björck, S., Kolstrup, E., Lemdahl, G. & Norberg, K.
802   1994: Late Weichselian environmental change in southern Sweden and
803   Denmark. *Journal of Quaternary Science 9*, 127-132.
804 Birks, H. H., Aarnes, I., Bjune, A. E., Brooks, S. J., Bakke, J., Kühl, N. & Birks, H. J. B.
805   2014: Lateglacial and early-Holocene climate variability reconstructed
806   from multi-proxy records on Andoya, northern Norway. *Quaternary*
807   *Science Reviews 89*, 108-122.
808 Birks, H. H., Battarbee, R. W. & Birks, H. J. B. 2000: The development of the
809   aquatic ecosystem at Kråkenes Lake, western Norway, during the late
810   glacial and early Holocene - a synthesis. *Journal of Paleolimnology 23*, 91-
811   114.
812 Birks, H. H. & Birks, H. J. B. 2014: To what extent did changes in July temperature
813   influence Lateglacial vegetation patterns in NW Europe? *Quaternary*
814   *Science Reviews 106*, 262-277.
815 Björck, S. 1979: *Weichselian stratigraphy of Blekinge, SE Sweden, and water level*
816   *changes in the Baltic Ice Lake*. Lund University. *LUNDQUA Thesis 7*, 248 pp.
817 Björck, S. 1981: A stratigraphic study of Late Weichselian deglaciation, shore
818   displacement and vegetation history in south-eastern Sweden. *Fossils and*
819   *Strata 14*, 1-93.
820 Björck, S. 1984: Bio- and chronostratigraphic significance of the Older Dryas
821   Chronozone - on the basis of new radiocarbon dates. *Geologiska*
822   *Föreningen i Stockholm Förhandlingar 106*, 81-91.
823 Björck, S. 1995: A review of the history of the Baltic Sea 13,0 to 8,0 ka BP:
824   *Quaternary International 27*, 19-40.
825 Björck, S., Kromer, B., Johnsen, S., Bennike, O., Hammarlund, D., Lemdahl, G.,
826   Possnert, G., Rasmussen, T. L., Wohlfarth, B., Hammer, C. U. & Spurk, M.
827   1996: Synchronised terrestrial-atmospheric deglacial records around the
828   North Atlantic. *Science 274*, 1155-1160.
829 Björck, S. & Möller, P. 1987: Late Weichselian environmental history in
830   southeastern Sweden during the deglaciation of the Scandinavian ice
831   sheet. *Quaternary Research 28*, 1-37.
832 Björck, S., Walker, M. J. C., Cwynar, L. C., Johnsen, S., Knudsen, K.-L., Lowe, J. J.,
833   Wohlfarth, B. & INTIMATE group members 1998: An event stratigraphy
834   for the Last Termination in the North Atlantic region based on the

835   Greenland ice-core record: a proposal by the INTIMATE group. *Journal of*
836   *Quaternary Science 13*, 283-292.

837 Blaauw, M. 2012: Out of tune: the dangers of aligning proxy archives. *Quaternary*
838   *Science Reviews 36*, 38-49.

839 Blaauw, M. & Christen, J. A. 2011: Flexible paleoclimate age-depth models using
840   an autoregressive gamma process. *Bayesian Analysis 6*, 457-474.

841 Blockley, P. E., Lane, C. S., Hardiman, M., Rasmussen, S. O., Seierstad, I. K.,
842   Steffensen, J. P., Svensson, A., Lotter, A. F., Turney, C. S. M., Bronk Ramsey,
843   C. & INTIMATE group members 2012: Synchronisation of
844   paleoenvironmental records over the last 60,000 years, and an extended
845   INTIMATE event stratigraphy to 48,000 b2k. *Quaternary Science Reviews*
846   *36*, 2-10.

847 Blunier, T. & Brook, E. J. 2001: Timing of millennial-scale climate change in
848   Antarctica and Greenland during the last glacial period. *Science 291*, 109-
849   112.

850 Broecker, W. S. 1998: Paleocean circulation during the last deglaciation: a bipolar
851   seesaw? *Paleoceanography 13*, 119-121.

852 Bronk Ramsey, C. 2010: *OxCal Program, v.4.1.7*. Radiocarbon accelerator unit,
853   University of Oxford, UK.

854 Brooks, S. J. & Langdon, P. G. 2014: Summer temperature gradients in northwest
855   Europe during the Lateglacial and early Holocene (15-8 ka BP) inferred
856   from chironomid assemblages. *Quaternary International 341*, 80-90.

857 Davies, S. M., Wastegård, S. & Wohlfarth, B. 2003: Extending the limits of the
858   Borrobol Tephra to Scandinavia and detection of new early Holocene
859   tephra. *Quaternary Research 59*, 345-352.

860 Davies, S. M., Wohlfarth, B., Wastegård, S., Andersson, M., Blockley, S. & Possnert,
861   G. 2004: Were there two Borrobol Tephras during the early Lateglacial
862   period: implications for tephrochronology? *Quaternary Science Reviews*
863   *23*, 581-589.

864 Digerfeldt, G. 1971: The Post-Glacial development of the ancient lake at
865   Torreberga, South Sweden. *Geologiska Föreningens i Stockholm*
866   *Förhandlingar 93*, 601-624.

867 Engstrom, D. R., Fritz, S. C., Almendinger, J. E. & Juggins, S. 2000: Chemical and
868   biological trends during lake evolution in recently deglaciated terrain.
869   *Nature 408*, 161-166.

870 EPICA, Community Members 2006: One-to-one coupling of glacial climate
871   variability in Greenland and Antarctica. *Nature 444*, 195-198.

872 Ising, J. 1998: Late Weichselian pollen stratigraphy, clay-varve chronology,
873   radiocarbon chronology, and palaeomagnetic secular variations at
874   Farslycke, Blekinge, southern Sweden. *GFF 120*, 321-332.

875 Iversen, J. 1954: The Late-Glacial flora of Denmark and its relation to climate and
876   soil. *Danmarks Geologiske Undersogelse II, 80*, 87-119.

877 Jackson, S. T. & Overpeck, J. T. 2000: Responses of plant populations and
878   communities to environmental changes of the Late Quaternary.
879   *Paleobiology 26*, 194-220.

880 Juggins, S. 2013: Quantitative reconstructions in palaeolimnology: new paradigm
881   or sick science? *Quaternary Science Reviews 64*, 20-23.

882 Karlatou-Charalampopoulou, A. 2016: *Vegetation responses to Late Glacial*
883   *climate shifts as reflected in a high-resolution pollen record from Blekinge,*

south-eastern Sweden, compared with responses of other climate proxies. M. Sc. thesis 464, Lund University, 17 pp.

Knutti, R., Flückiger, J., Stocker, T. F. & Timmermann, A. 2004: Strong hemispheric coupling of glacial climate through freshwater discharge and ocean circulation. *Nature 430*, 851-856.

Kolstrup, E. 1979: Herbs as July temperature indicators for parts of the pleniglacial and late-glacial in The Netherlands. *Geologie en Mijnbouw 58*, 377-380.

Kolstrup, E. 1980: Climate and stratigraphy in northwestern Europe between 30.000 B.P. and 13,000 B.P., with special reference to the Netherlands. *Mededelingen Rijks Geologische Dienst 32-15*, 181-253.

Kylander, M. E., Klaminder, J., Wohlfarth, B. & Löwemark, L. 2013: Geochemical responses to paleoclimatic changes in southern Sweden since the late glacial: the Hässeldala Port lake sediment record. *Journal of Paleolimnology 50*, 57-70.

Lane, C. S., Brauer, A., Blockley, S. P. E. & Dulski, P. 2013: Volcanic ash reveals time-transgressive abrupt climate change during the Younger Dryas. *Geology 41*, 1251-1254.

Lohne, Ø. S., Mangerud, J. & Birks, H. H. 2013: Precise ^{14}C ages of the Vedde and Saksunarvatn ashes and the Younger Dryas boundaries from western Norway and their comparison with the Greenland Ice Core (GICC05) chronology. *Journal of Quaternary Science 28*, 490-500.

Lohne, Ø. S., Mangerud, J. & Birks, H. H. 2014: IntCal13 calibrated ages of the Vedde and Saksunarvatn ashes and the Younger Dryas boundaries from Kråkenes, western Norway. *Journal of Quaternary Science 29*, 506-507.

Lowe, J. J., Rasmussen, S. O., Björck, S., Hoek, W. Z., Steffensen, J. P., Walker, M. J. C., Yu, Z. & INTIMATE group members 2008: Synchronisation of palaeoenvironmental events in the North Atlantic region during the Last Termination: a revised protocol recommended by the INTIMATE group. *Quaternary Science Reviews 27*, 6-17.

Lowe, J. J., Bronk Ramsey, C., Housley, R., Lane, C. S. & Tomlinson, E. 2015: The RESET project: constructing a European tephra lattice for refined synchronisation of environmental and archaeological events during the last c. 100 ka. *Quaternary Science Reviews 118*, 1-17.

Lundqvist, J. & Wohlfarth, B. 2001: Timing and east-west correlation of south Swedish ice marginal lines during the Late Weichselian. *Quaternary Science Reviews 20*, 1127-1148.

Mangerud, J., Andersen, S. T., Berglund, B. E. & Donner, J. J. 1974: Quaternary stratigraphy of Norden, a proposal for terminology and classification. *Boreas 3*, 109-128.

Matthews, I. P., Birks, H. H., Bourne, A. J., Brooks, S. J., Lowe, J. J., MacLoed, A. & Pyne-O'Donnell, S. D. F. 2011: New age estimates and climatostratigraphic correlations for the Borrobol and Penifiler Tephras: evidence from Abernethy Forest, Scotland. *Journal of Quaternary Sciences 26*, 247-252.

Möller, P. 1987: Moraine morphology, till genesis, and deglaciation pattern in the Åsnen area, south-central Småland, Sweden. *LUNDQUA Thesis 20*, 146 pp.

Muscheler, R., Adolphi, F. & Knudsen, M.F. 2014: Assessing the differences between the IntCal and Greenland ice-core time scales for the last 14,000 years via the common cosmogenic radionuclide variations. *Quaternary*

Science Reviews 106, 81–87.

Muschitiello, F., Andersson, A., Wohlfarth, B. & Smittenberg, R. H. 2015a: The C_{20} highly branched isoprenoid biomarker – A new diatom-sourced proxy for summer trophic conditions? *Organic Geochemistry 81*, 27-33.

Muschitiello, F., Pausata, F. S. R., Smittenberg, R. H., Salih, A. A. M., Watson, J. E., Brooks, S. J., Whitehouse, N. J., Karlatou-Charalampopoulou, A. & Wohlfarth, B. 2015b: Fennoscandian freshwater control on Greenland hydrological shifts at the onset of the Younger Dryas. *Nature Communications* 6, 8939.

Muschitiello, F. & Wohlfarth, B. 2015: Time-transgressive environmental shifts across Northern Europe at the onset of the Younger Dryas. *Quaternary Science Reviews 109*, 49-56.

Pearce, C., Seidenkrantz, M. S., Kuijpers, A., Massé, G. & Reynisson, N. F. 2013: Ocean lead at the termination of the Younger Dryas cold spell. *Nature Communications 4*, p. 1664.

Pyne-O'Donnell, S. D. F. 2010: The taphonomy of Last Glacial–Interglacial Transition (LGIT) distal volcanic ash in small Scottish lakes. *Boreas 40*, 131-145.

Pyne-O'Donnell, S. D. F., Blockley, S. P. E., Turney, C. S. M. & Lowe, J. J. 2008: Distal volcanic ash layers in the Lateglacial Interglacial (GI-1): problems of stratigraphic discrimination. *Quaternary Science Reviews 27*, 72-84.

Rach, O., Brauer, A., Wilkes, H. & Sachse, D. 2014: Delayed hydrological response to Greenland cooling at the onset of the Younger Dryas in western Europe. *Nature Geoscience 7*, 109-112.

Rasmussen, S. O., Bigler, M., Blockley, S. P. E., Blunier, T., Buchardt, S. L., Clausen, H. B., Cvijanovic, I., Dahl-Jensen, D., Johnsen, S. J., Fischer, H., Gkinis, V., Guillevic, M., Hoek, W. Z., Lowe, J. J., Pedro, J., Popp, T., Seierstad, I. K., Steffensen, J. P., Svensson, A. M., Vallelonga, P., Vinther, B. M., Walker, M. J. C., Wheatley, J. J. & Winstrup, M. 2014: Stratigraphic framework for robust naming and correlation of abrupt climatic changes during the last glacial period based on three synchronized Greenland ice core records. *Quaternary Science Reviews 106*, 14-28.

Reimer, P. J., Bard, E., Bayliss, A., Warren Beck, J. W., Blackwell, P. G., Bronk Ramsey, C., Buck, C. E., Cheng, H., Lawrence Edwards, R. L., Friedrich, M., Grootes, P. M., Haflidason, H., Hajdas, I., Hatté, C., Heaton, T. J., Hoffmann, D. L., Hogg, A. G., Hughen, K. A., Kaiser, K. F., Kromer, B., Manning, S. W., Niu, M., Reimer, R. W., Richards, D. A., Scott, E. M., Southon, J. R., Staff, R. A., Turney, C. S. M. & van der Plicht, J. 2013: INTCAL13 and MARINE13 Radiocarbon age calibration curves 0–50,000 years cal BP. *Radiocarbon 55*, 1869–1887.

Ringberg, B. 1991: Late Weichselian clay varve chronology and glaciolacustrine environment during deglaciation in southeastern Sweden. *Sveriges Geologiska Undersökning 79*, 1-42.

Steffensen, J. P., Andersen, K. A., Bigler, M., Clausen, H. B., Dahl-Jensen, D., Fischer, H., Goto-Azuma, K., Hansson, M., Johnsen, S. J., Jouzel, J., Masson-Delmotte, V., Popp, T., Rasmussen, S. O., Röthlisberger, R., Ruth, U., Stauffer, B., Siggaard-Andersen, M. L., Sveinbjörnsdóttir, A. E., Svensson, A. and White, J. W. C. 2008: High-resolution Greenland ice core data show abrupt climate change happens in few years. *Science 321*, 680-684.

982   Steinthorsdottir, M., de Boer, A., Oliver, K. I. C., Muschitiello, F., Blaauw, M.,
983   Reimer, P. J. & Wohlfarth, B. 2014: Synchronous records of pCO$_2$ and Δ^{14}C
984   suggest rapid, ocean-driven pCO$_2$ fluctuations at the onset of Younger
985   Dryas. *Quaternary Science Reviews 99*, 84-96.
986   Steinthorsdottir, M., Wohlfarth, B., Kylander, M., Blaauw, M. and Reimer, P. J.
987   2013: Stomatal proxy record of CO$_2$ concentrations from the Last
988   Termination suggests an important role for CO$_2$ at climate change
989   transitions. *Quaternary Science Reviews 68*, 43-58.
990   Stocker, T. F. & Johnsen, S. J. 2003: A minimum thermodynamic model for the
991   bipolar seesaw. *Paleoceanography 18*, 1944-9186.
992   Walker, M. J. C., Björck, S., Lowe, J. J., Cwynar, L. C., Johnsen, S., Knudsen, K.-L.,
993   Wohlfarth, B. & INTIMATE group members 1999: Isotopic 'events' in the
994   GRIP ice core: a stratotype for the Late Pleistocene. *Quaternary Science
995   Reviews 18*, 1143-1150.
996   Walker, M. J. C., Lowe, J. J., Blockley, S. P., Bryant, C., Coombes, P., Davies, S. M.,
997   Hardiman, M., Turney, C. S. M. & Watson, J. 2012: Lateglacial and early
998   Holocene palaeoenvironmental 'events' in Sluggan Bog, Northern Ireland:
999   comparisons with the Greenland NGRIP GICC05 event stratigraphy.
1000   *Quaternary Science Reviews 36*, 124-138.
1001   Watson, J. 2008: *Quantifying Late Glacial climate change in Northwestern Europe
1002   using two insect proxies*. Ph. D. thesis, The Queen's University of Belfast,
1003   365 pp.
1004   Wohlfarth, B. 1996: The chronology of the Last Termination: a review of high-
1005   resolution terrestrial stratigraphies. *Quaternary Science Reviews 15*, 267-
1006   284.
1007   Wohlfarth, B., Björck, S., Lemdahl, G. & Ising, J. 1994: Ice recession and
1008   depositional environment in the Blekinge archipelago of the Baltic Ice
1009   Lake. *GFF 116*, 3-12.
1010   Wohlfarth, B., Blaauw, M., Davies, S. M., Andersson, M., Wastegård, S., Hormes, A.
1011   & Possnert, G. 2006: Constraining the age of Lateglacial and early
1012   Holocene pollen zones and tephra horizons in southern Sweden with
1013   Bayesian probability methods. *Journal of Quaternary Science 21*, 321-334.
1014   Wohlfarth, B. & Possnert, G. 2000: AMS radiocarbon measurements from
1015   Swedish varved clays. *Radiocarbon 42*, 323-333.

1016

1017

1018

1019

1020   Figure captions

1021

1022   *Figure 1.* A. Location of the study area in southern Sweden. B. Topography

1023   around Hässeldala Port's peatbog. C. Close-up of Hässeldala Port's peatbog

1024   showing the location of the cored successions (see Table 1 for details on the

1025   different sequences). All studied profiles were derived from the deepest part of

1026   the bog. Present-day lakes are shown in blue and peat bogs in a light brown

1027   colour. Elevations around Hässeldala Port reach between 35 and 80 m above

1028   present day sea level (a.s.l.).

1029

1030   *Figure 2.* Lithostratigraphy, total organic carbon (TOC) and loss-on-ignition (LOI)

1031   for Hässeldala Port's core #2 (Wohlfarth *et al.* 2006) and #5 (Steinthorsdottir *et*

1032   *al.* 2013). The brown and grey shaded rectangles mark the distinct patterns that

1033   can be recognised in all profiles. See Fig. 1C for the location of the cores.

1034   *Figure 3.* A. TOC/LOI (%) curves for cores #1, #2, #3, #HP4, #5, and #6 according

1035   to depth. The brown and grey shaded rectangles mark the distinct patterns that

1036   can be recognised in all profiles. See Table 1 for references for each analysed

1037   sediment core. B. TOC/LOI (%) curves for cores #1, #2, #3, #HP4, #5, and #6

1038   shown on the revised chronology for core #5 (Muschitiello *et al.* 2015b) (see text

1039   and Fig. 4). The grey shaded area shows those parts of the profiles, where the age

1040   was interpolated using known sedimentation rates. Tephra layers that have been

1041   geochemically identified are the Askja-S tephra (AsT), the Hässeldala tephra

1042   (HDT) and the Borrobol tephra (BT) (Davies *et al.* 2003, 2004; Wohlfarth *et al.*

1043   2006), while other tephras in core #1 and #HP4 have not been further analysed.

1044   None of these tephras has been used in the construction of the age model.

1045

1046   *Figure 4.* Age model of Hässeldala Port's composite radiocarbon-dated

1047   succession using the IntCal13 calibration curve (Reimer *et al.* 2013). Circles

1048   indicate calibrated ^{14}C dates used to construct the age model. Blue colored circles

1049   refer to dates that were transferred from core #2 onto core #5's depth scale. The

1050   orange dotted lines show the 95% confidence bounds of the model, and the red

1051   dotted line the modelled weighted mean age. See Table 3 for details on all [14]C

1052   dates.

1053   *Figure 5.* Shoreline displacement and relative timing of the deglaciation in

1054   Blekinge province, southernmost Sweden during the regional Bølling and Older

1055   Dryas pollen zones. See Table 5 for details of all sites shown here. A. Ice

1056   recession lines (white dashed line) according to the stacked local clay-varve

1057   chronology (Ringberg 1991). The formation of the highest coastline of the Baltic

1058   Ice Lake estimated at 65-67 m a.s.l. (blue line) corresponds approximately to

1059   local varve years -10 to +10, i.e. to a position of the active ice margin around

1060   Farslycke and sites 171 and 172. The white shaded part shows the extension of

1061   the former ice sheet. B. Ice recession lines (white dashed line) according to the

1062   stacked local clay-varve chronology (Wohlfarth *et al.* 1994). The shoreline at 50-

1063   55 m a.s.l. (orange line) formed coincident with the deposition of the thick varves

1064   (local varve years +88 to +220). By this time, the active ice margin was located to

1065   the north of the study region, but stagnant ice remained above the highest

1066   coastline (Björck & Möller 1987). C. Land uplift around Hässeldala Port during

1067   the last deglaciation and location of the site in respect to the former coastlines of

1068   the Baltic Ice Lake. A. The coastline at 50-55 m a.s.l. (orange line) corresponds to

1069   the end of the regional Bølling pollen zone. D. The coastline at 45-50 m a.s.l.

1070   (dark green line) corresponds to the regional Older Dryas pollen zone. During

1071   the early part of the regional deglaciation Hässeldala Port was situated in an

1072   archipelago in the Baltic Ice Lake, but soon became part of a more continuous

1073   land area.

1074

1075   *Figure 6.* Hässeldala Port's lithostratigraphy and multi-proxy records shown on

1076   the revised chronology of core #5. A. Simplified lithostratigraphy of core #5. The

1077   lowermost unit 1 was only present in cores #1-3 and HP4 (see Figs 2 and 3A, B

1078   for details) and has been interpolated to core #5. B. Loss-on-ignition (LOI) curve

1079   for core #5. C. Reconstructed pH, diatom assemblage zones (DAZ-I to DAZ-IV)

1080   and crysophyte:diatom (C:D) ratios for core #5 (Ampel *et al.* 2014). D. Leaf-wax

1081   derived hydrogen isotope parameters for aquatic ($\delta D_{n\text{-}C_{21}}$) and terrestrial plants

1082   ($\delta D_{n\text{-}C_{27\text{-}29\text{-}31}}$) and calculated terrestrial evaporation ($\Delta\delta D_{terr\text{-}aq}$) for core #5

1083   (Muschitiello *et al.* 2015b). All proxies in B-D were analysed on the same split

1084   samples. E. Chironomid-derived mean summer surface water temperatures for

1085   core #HP4 (Watson 2008) are shown on the revised core #5 chronology. F.

1086   Geochemically determined cryptotephra layers (AsT = Askja-S tephra; HDT =

1087   Hässeldala tephra; BT = Borrobol tephra) in cores #1-3 (Davies *et al.* 2003; 2004;

1088   Wohlfarth *et al.* 2006) are shown on the timescale of core #5 using the core-to-

1089   core alignment described in the text. G. The presence/absence of charcoal and of

1090   *Betula pubescens* and *Pinus sylvestris* macrofossils in core #2 is here shown on

1091   the timescale of core #5. H. Local pollen assemblage zones (HÄP-1 to HÄP-7) of

1092   core #3 (Andersson 2004; Wohlfarth *et al.* 2006) plotted on the revised core #5

1093   chronology. I. Local pollen assemblage zones of core #6 (Karlatou-

1094   Charalampopoulou 2016) plotted on the revised core #5 chronology. J. Regional

1095   pollen zones (Björck & Möller 1987) and inferred Lateglacial and early Holocene

1096   vegetation in southern Sweden.

1097

1098   *Figure 7.* Age estimates for Allerød-Younger Dryas pollen zone transitions (one

1099   sigma) inferred from well-dated North European pollen stratigraphic sites

1100   (green bars): Kråkenes (Birks *et al*. 2000); Madtjärn (Björck *et al.* 1996); Sluggan

1101   Bog (Walker *et al.* 2012) and Meerfelder Maar (Rach *et al.* 2014). The age of the

1102   local pollen zone Hä-3 (brown bar) in Hässeldala Port (Karlatou-

1103   Charampopoulou 2016), which is a transitional zone between the regional

1104   Allerød and Younger Dryas pollen zones, is shown for comparison. Age estimates

1105   for the onset of Greenland Interstadial 1a (GI-1a) and Greenland Stadial 1 (GS-1)

1106   are expressed on the IntCal13 time scale after synchronization with the GICC05
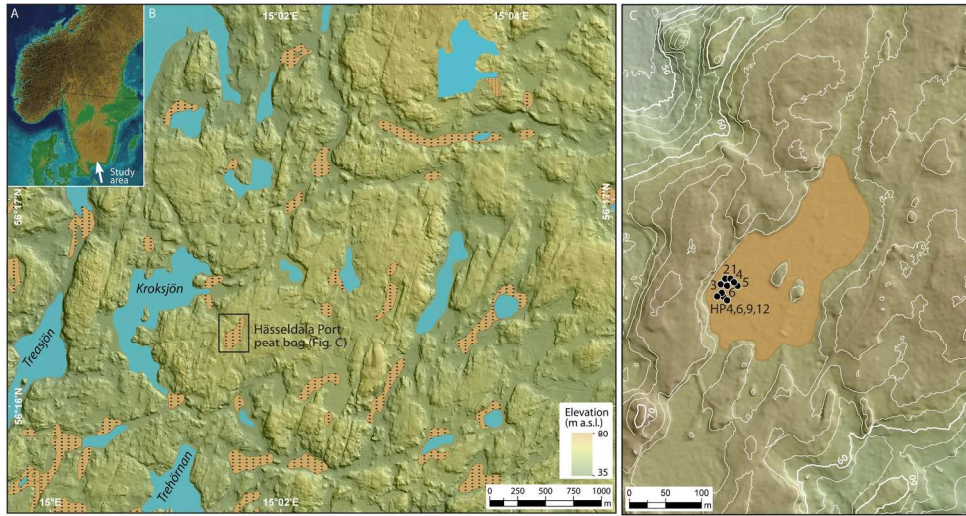
1107   scale (Muscheler *et al.* 2014).

1108   *Figure 8.* Comparison of Lateglacial and early Holocene vegetation and

1109   hydroclimate changes as reconstructed from Hässeldala Port (HÄ) (Muschitiello

1110   *et al.* 2015b) and Meerfelder Maar (MFM) (Rach *et al.* 2014) compared to the

1111   Greenland event stratigraphy (displayed and plotted on the IntCal13 time scale -

1112   Muscheler *et al.* 2014). The red star marks the position of the Vedde Ash in

1113   Meerfelder Maar and in the NGRIP ice core.

1114

1
2
3   1115
4
5   1116
6
7
8
9
10
11
12
13
14
15
16
17
18
19
20
21
22
23
24
25
26
27
28
29
30
31
32
33
34
35
36
37
38
39
40
41
42
43
44
45
46
47
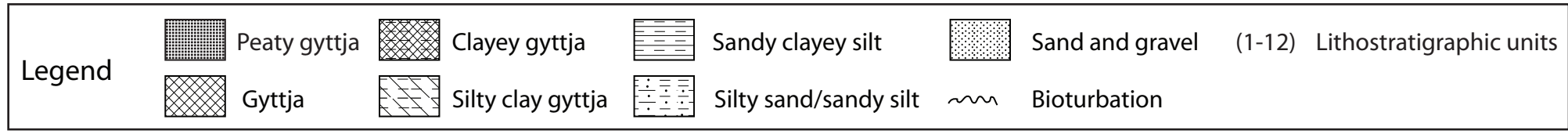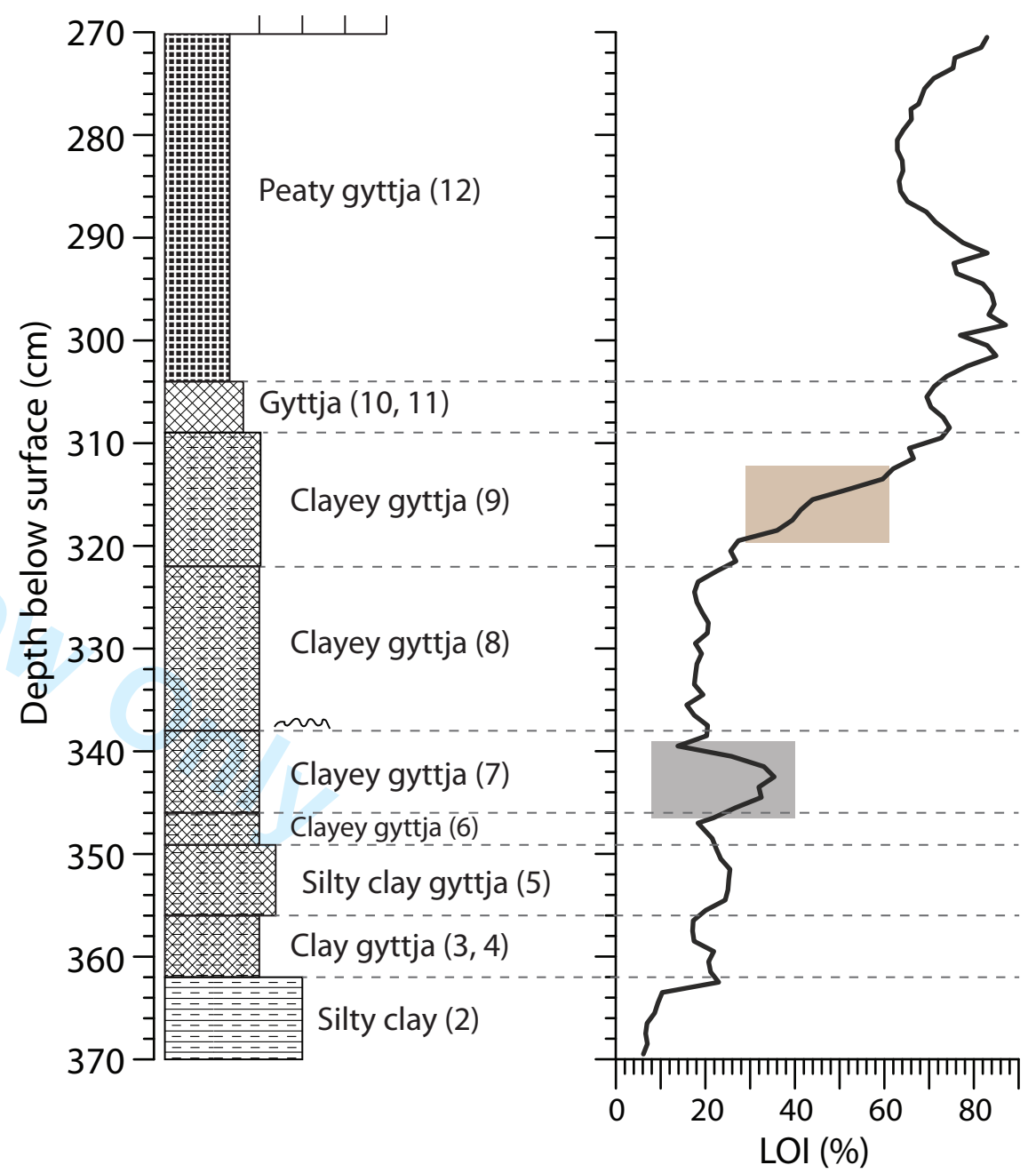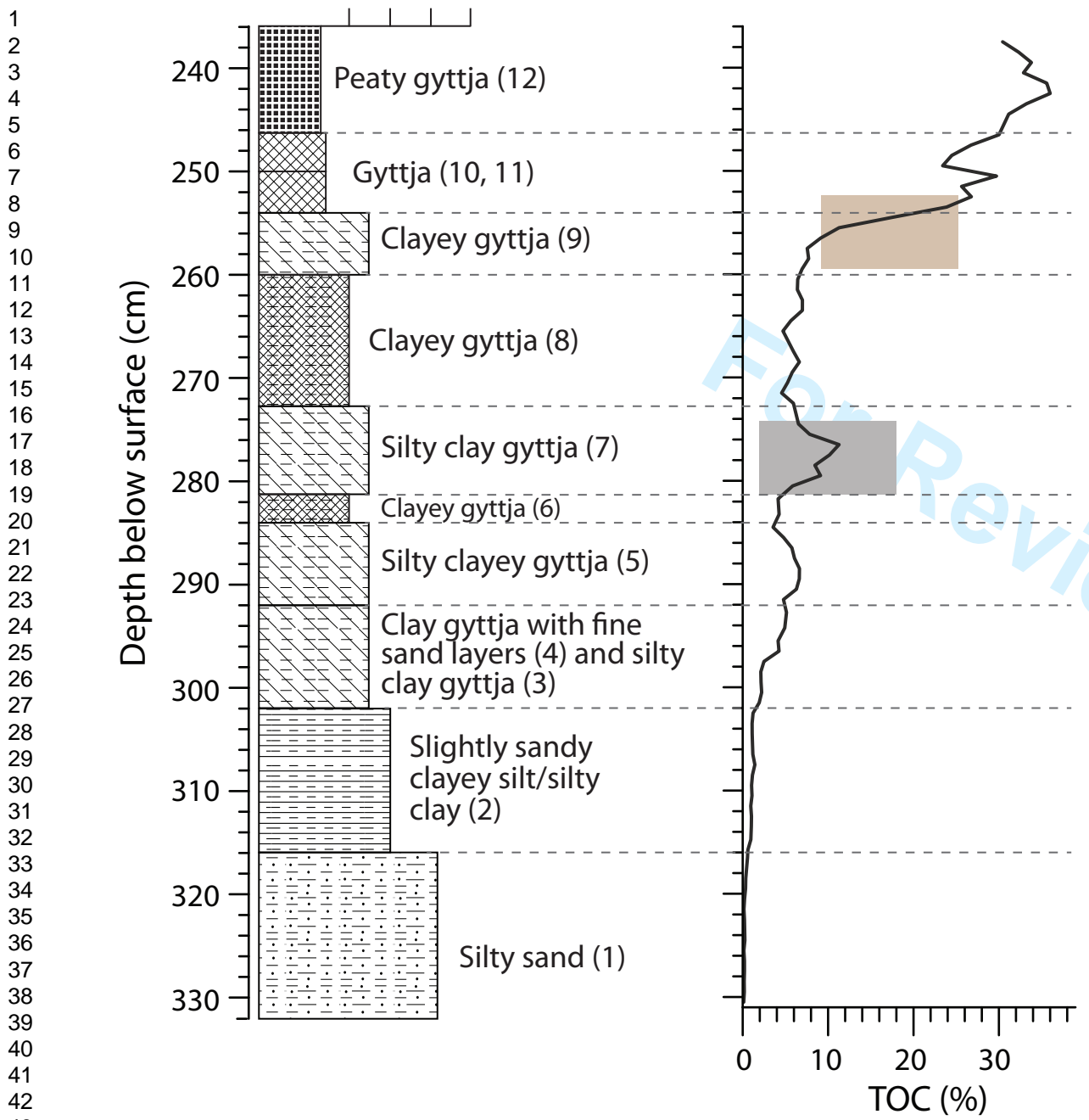48
49
50
51
52
53
54
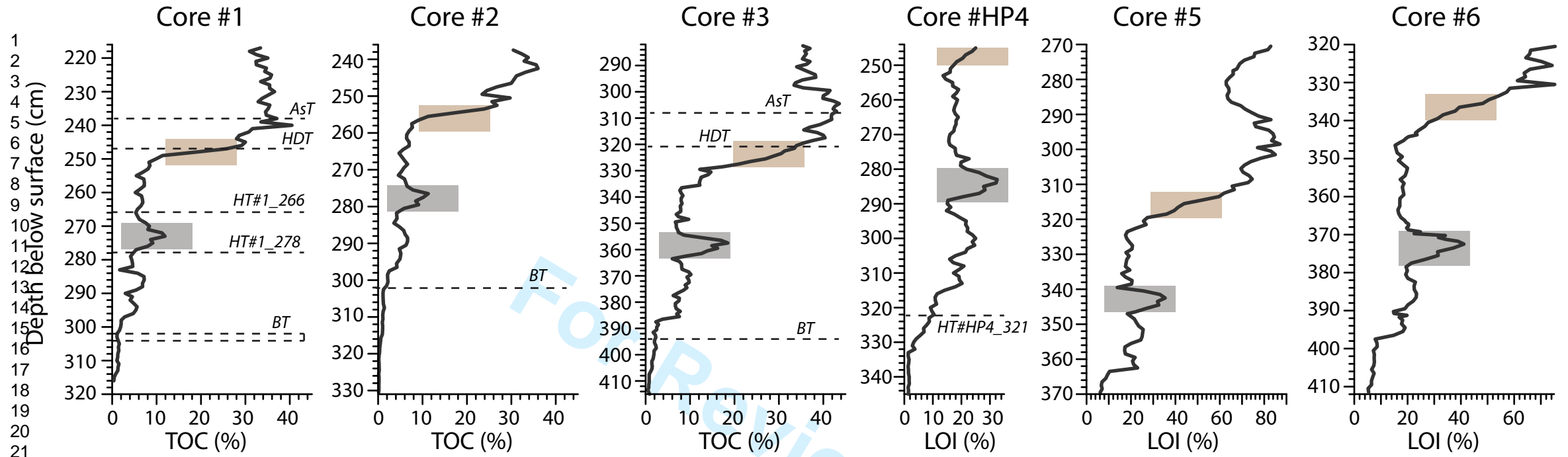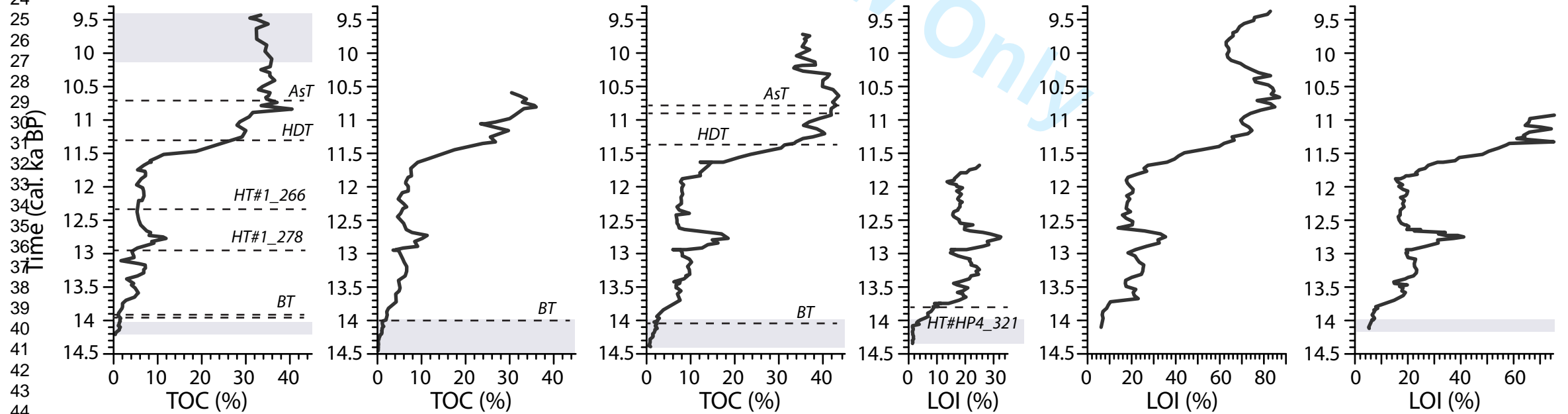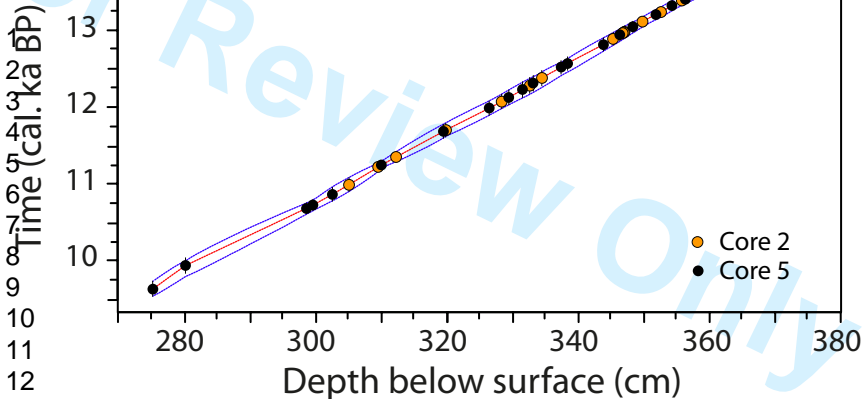55
56
57
58
59
60

168x91mm (300 x 300 DPI)

Boreas

Core #2

Core #5

A

Core #1 | Core #2 | Core #3 | Core #HP4 | Core #5 | Core #6

B

Boreas

288x283mm (300 x 300 DPI)

A

Dark brown peaty gyttja (12)

Dark brown gyttja (11)

Brown gyttja (10, 9)

Light brown gyttja clay/ clayey gyttja and brown clayey silty gyttja (8a-c)

Dark brown clayey gyttja (7)

Brown clayey gyttja/gyttja clay (6-3)

Silty clay (2)

Silty fine sand (1)

Time (cal. ka BP)

Hässeldala Port - Core #5

Boreas

B

C

DAZ-IV
DAZ-III
DAZ-II
DAZ-I

D

Drier
Wetter
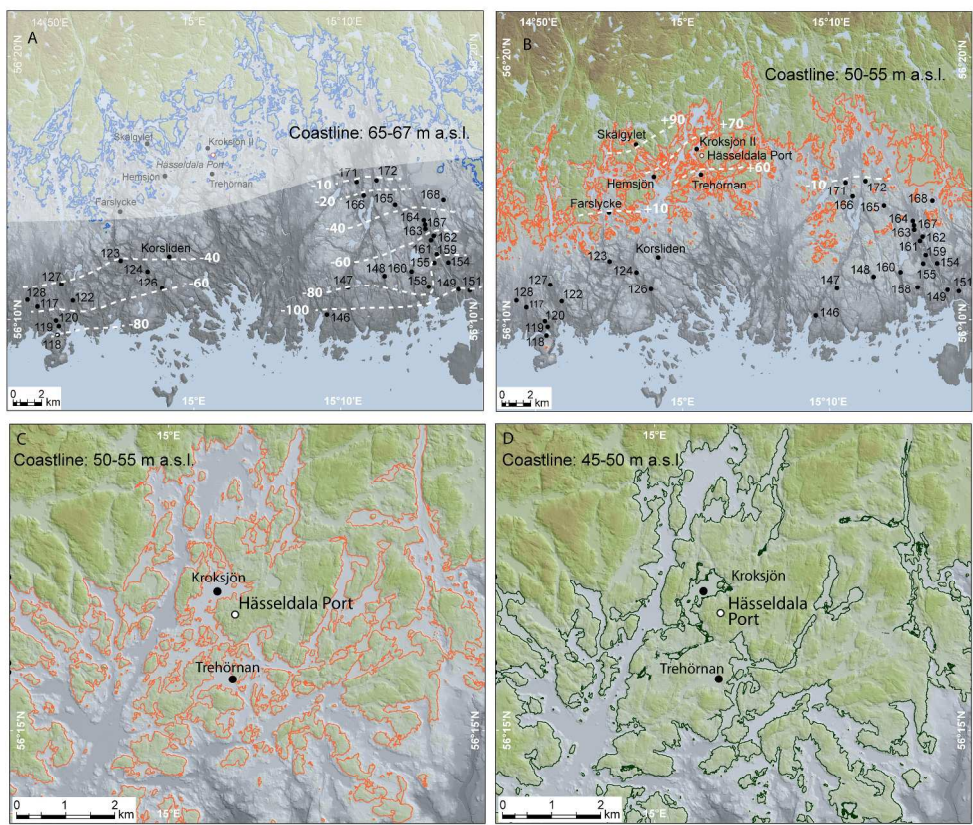
Core #HP4 on core #5 time scale

E

Cores #2 and 3 on core #5 time scale

F

AsT
HDT
'BT'

G

Pinus sylvestris
Betula pubescens

H

HÄP-7
HÄP-6
HÄP-5
HÄP-4
HÄP-3
HÄP-2
HÄP-1

Core #6 on core #5 time scale

I

Hä-6
Hä-5
Hä-4
Hä-3
Hä-2
Hä-1

Regional pollen zones and vegetation

J

Open forests
Grasses, herbs, shrubs and dwarf shrubs

Holocene
Younger Dryas
Alleröd II
Alleröd I
Older Dryas

Time (cal. ka BP)

LOI (%)
pH
C:D ratio
δD n-C21 (⁰/₀₀)
ΔδDterr-aq (⁰/₀₀)
Mean Tjuly (°C)
Tephra
Charcoal present
Tree macrofossils present
Local pollen zones
Local pollen zones

Allerød - Younger Dryas pollen zone transition

Kråkenäs (K)
Madtjärn (M)
Hässeldala Port (HÄ)
Meerfelder Maar (MFM)
Sluggan Bog (SB)

Onset of GS-1
Onset of GI-1a

North Sea

500 km

Greenland Event Stratigraphy

12.6   12.8   13.0   13.2
Time (cal. ka BP)

HÄ Hässeldala   ⭐ Vedde Ash   GS Greenland stadial
MFM Meerfelder Maar   ╱ 50-a moving average   GI Greenland interstadial
YD Younger Dryas

Table 1. Hässeldala Port sedimentary successions and analysed proxies. LOI = loss-on-ignition; TOC = total organic carbon; C/N = carbon:nitrogen ratio; XRF = major elements. Watson (2008) obtained a total of 14 parallel sediment cores from Hässeldala and sampled six of these for coleoptera analysis, two for tephra, four for LOI, and one for chironomids (#HP4). Correlation between these cores was based on stratigraphic correlations and on the pattern of the respective LOI curves (Watson 2008). See Fig. 1C for the location of the various cores.

Core #	Proxy	Reference
1	LOI, TOC, tephra	Davies *et al.* (2003)
2	TOC, tephra, ^{14}C	Davies *et al.* (2004)
3	TOC, tephra, pollen stratigraphy	Davies *et al.* (2004); Andersson (2004), Wohlfarth *et al.* (2006)
4	TOC, C/N, $\delta^{13}C_{bulk}$, $\delta^{15}N_{bulk}$, XRF	Kylander *et al.* (2013)
HP4	LOI, tephra, chironomids	Watson (2008), Muschitiello *et al.* (2015b)
HP6	LOI	Watson (2008)
HP9	LOI, tephra	Watson (2008)
HP12	LOI	Watson (2008)
5	LOI, ^{14}C, leaf stomata	Steinthorsdottir *et al.* (2013, 2014)
	Diatoms	Ampel *et al.* (2014)
	XRF	Unpublished
	Biomarkers	Muschitiello *et al.* (2015a, b)
	δD_{wax}, $\delta^{13}C$	Muschitiello *et al.* (2015b)
6	LOI, pollen stratigraphy	Muschitiello *et al.* (2015b); Karlatou-Charalampopoulou (2016)

Table 2. Cryptotephra found in Hässeldala Port's sediments (Davies *et al.* 2003, 2004) and Watson (2008). The Askja-S tephra (AsT), the Hässeldala tephra (HDT) and the Borrobol tephra (BT) have been geochemically identified in cores #1, 2 and 3 (Davies *et al.* 2003, 2004). Other cryptotephra layers found in cores #1 and HP4 could not be geochemically identified. See Fig. 1C for the location of the cores and Fig. 3A for details on the position of the individual tephra horizons. Tephra shard concentrations peak in core #1 at 304-303 cm depth, but remain high as far as 301 cm depth. Note that Matthews *et al.* (2011) suggested that Hässeldala Port's BT is younger than the BT found in Scotland and likely an equivalent to the Penifiler tephra.

Cryptotephra	Core #1 depth (cm)	Core #2 depth (cm)	Core #3 depth (cm)	Core #HP4 depth (cm)
Askja-S (AsT)	HT#1_238		HT#3_308-310	
Hässeldala (HDT)	HT#1_247		HT#3_ 321-322	
NN	HT#1_266			
NN	HT#_278			
NN				HT#HP4_321
Borrobol (BT)	HT#1_304-303 (302-301)	HT#2_302	HT#3_394	

Table 3. AMS ¹⁴C dates for Hässeldala Port based on selected terrestrial plant remains and used to construct the composite age-depth model (Wohlfarth *et al.* 2006; Muschitiello *et al.* 2015b). Sample ID's shown in italics refer to dates that were transferred from core #2 to core #5 (see Fig. 4). However not all of these were used to construct the age model, since some of the ¹⁴C dates were clear outliers. B = *Betula nana* – leaves, leaf fragments, seeds, buds, twigs; Bi = *Betula* indet. – twigs, leaf fragments, seeds, bark; Bp = *Betula pubescens* – seeds; C = charcoal; D = *Dryas octopetala* – leaves, leaf fragments, seeds, buds; M = moss; P = *Pinus sylvestris* – needles; T = undetermined terrestrial material. The sample depth refers to core #5 and the depth shown in brackets refers to the original depth in core #2 (Wohlfarth *et al.* 2006).

Sample depth (cm)	Thickness error (cm)	Sample ID	Material analysed	¹⁴C age (a)	¹⁴C error (1 sigma)	Used in the age model
369.5	0.5	UBA-20296	B, D	12 211	57	Yes
367.5	0.5	UBA-20297	D, S	11 972	62	Yes
366.6 (298.45)	1.15	*Ua-20516*	B, D, T	12 355	190	No
365.25	0.75	UBA-20298	B, D, S	11 673	56	No
363	0.5	UBA-20299	B, D	11 819	57	Yes
362.65 (296.2)	1.4	*Ua-20517*	B, D	11 920	90	Yes
360.5	0.5	UBA-20300	B, D	11 735	60	Yes
360.15 (294.35)	0.75	*Ua-20518*	B, D	11 990	110	No
358.5	0.5	UBA-20301	B, D	11 614	55	Yes
358.4 (292.85)	0.95	*Ua-20519*	B	11 805	240	Yes
356.5	0.5	UBA-20302	B, D	11 565	56	Yes
356 (291)	1.1	*Ua-20520*	B	11 525	85	Yes
354.5	0.5	UBA-20303	B	11 515	65	Yes
352.85 (289)	1.2	*Ua-20521*	T	11 490	85	Yes
352	1	UBA-20304	B	11 225	60	Yes
350 (287)	1.25	*Ua-20522*	B	11 455	125	Yes
348.5	0.5	UBA-20305	B	11 118	60	Yes
347.25 (285)	1.2	*Ua-20523*	B, T	11 245	95	Yes
347.1 (283.25)	0.9	*Ua-20524*	B, T	11 275	95	Yes
346.95 (281.5)	1.05	*Ua-20525*	B	11 200	165	Yes
346.5	0.5	UBA-20306	B	10 998	63	Yes
345.5 (279.5)	1	*Ua-20526*	B, T	10 935	80	Yes
344	1	UBA-20307	B	10 894	63	Yes
339.9 (274.75)	1.8	*Ua-20527*	B, T	11 070	135	No
338.5	0.5	UBA-20308	B	10 644	58	Yes
337.5	0.5	UBA-20309	B	10 484	50	Yes
337.4 (272.1)	0.95	*Ua-20528*	B, T	10 935	80	No

334.55 (270.3)	0.95	*Ua-20529*	B, T	10 515	75	Yes
333.25	1.75	UBA-20310	B	10 331	51	Yes
332.7 (268.45)	1	*Ua-16740*	B	10 165	95	Yes
331.6	1.5	UBA-20311	B	10 301	57	Yes
329.5	0.5	UBA-23306	Bi	10 331	53	Yes
328.5	0.5	UBA-20312	B	10 639	51	No
328.4 (265.5)	1.05	*Ua-16745*	B, D	10 285	95	Yes
326.5	0.5	UBA-20313	B	10 130	69	Yes
323.35 (259.1)	1.15	*Ua-16747*	B	9860	85	No
319.85 (257)	1.15	*Ua-16750*	B, C	10 205	85	Yes
319.5	0.5	UBA-21574	B	10 102	67	Yes
315.9 (255)	1.1	*Ua-16752*	B, Bp, P	9720	90	No
312.25 (253)	1.1	*Ua-16761*	B, T	9955	90	Yes
310	1	UBA-22308	Bi, M	9864	47	Yes
309.5 (251)	1.15	*Ua-16766*	P	9765	85	Yes
305.05 (246.75)	1.15	*Ua-16768*	P	9625	70	Yes
302.5	0.5	UBA-21575	B	9532	59	Yes
299.5	0.5	UBA-21577	B	9442	52	Yes
298.5	0.5	UBA-21578	B	9416	47	Yes
290	1	UBA-21576	B, C	7496	55	No
280	1	UBA-23309	Bi	9129	50	Yes
275	0.5	UBA-21579	T	8605	46	Yes

Table 4. Core ID, core depth and modelled and estimated ages for each core from Hässeldala Port (see Fig. 1C for the location of the cores and Fig. 3A for their TOC/LOI profiles). The statistical alignment of the TOC/LOI profiles of cores #1-HP4 and #6 to core #5 using a Monte Carlo algorithm (Muschitiello *et al.* 2015a, b) allowed transferring the chronology of core #5 to each of the profiles (Fig. 3B). The sedimentation rate in the uppermost/lowermost layers in some of the profiles had to be estimated (see main text), because these parts did not overlap with core #5: [1] = sedimentation rate 23 a cm⁻¹; [2] = sedimentation rate 22 a cm⁻¹; [3] = sedimentation rate 16 a cm⁻¹.

Core ID	Core depth (cm)	Depth (cm) interval for which the age could be modelled by correlation to core #5	Modelled median age (cal. ka BP)	Depth (cm) interval for which the age was interpolated using sedimentation rates	Estimated ages (cal. ka BP)
#1	217-316			217-225[1]	9.4-10.1
		226-305	10.2-14.0		
				306-316[2]	14.0-14.2
#2	237-331	237.5-301.5	10.6-14.0		
				302.5-330.5[3]	14.0-14.5
#3	282-415	282.5-289.5	9.7-14.0		
				290.5-415[3]	14.0-14.4
#4	336-436	—	—	—	—
#HP4	245-345	245-329	11.7-14.0		
				330-345[2]	14.0-14.3
#5	270-370	278.5-369.5	9.8-14.1		
#6	320-412	320.5-410.5	10.9-14.1	410.5-411.5	14.1

Table 5. Clay-varve localities investigated in Blekinge province, southernmost Sweden (Björck 1981; Ringberg 1991; Wohlfarth *et al.* 1994; Ising 1998). The local varve year corresponds to the year when the respective site had become ice free and refers to the local varve chronology for Blekinge. The numbering of the sites follows Ringberg (1991). See Fig. 5A and B for the location of the sites.

Site #	Site name	Local varve year	References
146	Vieryd 1	-103	Ringberg (1991)
149	R Fornanäs 4	-102	Ringberg (1991)
151	R Angelskog 6	-100	Ringberg (1991)
154	R Folkets Hus 9	-86	Ringberg (1991)
155	R Persborg 10	-85	Ringberg (1991)
118	Sternö	-80	Ringberg (1991)
147	Hjälmseryd 2	-80	Ringberg (1991)
158	R Långkärra 13	-79	Ringberg (1991)
160	Torneryd 15	-79	Ringberg (1991)
148	Saxemara 3	-73	Ringberg (1991)
159	R Snäckebacken 14	-73	Ringberg (1991)
119	Munkahus	-72	Ringberg (1991)
120	Drösebro	-67	Ringberg (1991)
161	R Herstorp I 16	-65	Ringberg (1991)
162	R Silverforsen 17	-63	Ringberg (1991)
126	Skyekärr	-60	Ringberg (1991)
117	Stilleryd	-59	Ringberg (1991)
163	R Herstorp II 18	-52	Ringberg (1991)
128	Horsaryd	-49	Ringberg (1991)
167	R Sörby 22	-49	Ringberg (1991)
122	Gustafsborg	-48	Ringberg (1991)
124	Trensum	-48	Ringberg (1991)
164	R Herstorp III 19	-48	Ringberg (1991)
127	Karlshamn	-41	Ringberg (1991)
123	Häggarp	-41	Ringberg (1991)
	Korsliden	-39	Wohlfarth *et al.* (1994)
165	Kjettorp I 20	-37	Ringberg (1991)
168	Kallinge Järnvägen 23	-31	Ringberg (1991)
166	Trofta	-22	Ringberg (1991)
171	Härsjölund 26	-11	Ringberg (1991)
172	Tubbarp I 27	-11	Ringberg (1991)
	Farslycke	+10	Ising (1998)
	Trehörnan	+65	Wohlfarth *et al.* (1994)
	Hemsjön	+72	Wohlfarth *et al.* (1994)
	Kroksjön II	+77	Björck (1981), Wohlfarth *et al.* (1994)
	Skälgylet	+89	Wohlfarth *et al.* (1994)

Table 6. Plant species present in Blekinge, southernmost Sweden during the last glacial/interglacial transition according to pollen stratigraphic and plant macrofossil analyses (Björck 1981; Berglund 1966; Wohlfarth *et al.* 1994, 2006; Steinthorsdottir *et al.* 2013). Asterisk indicates finds of plant macrofossil remains.

Time interval	Plant species
>14.1 ka BP	*Artemisia, *Betula nana, *Betula pubescens, Calluna vulgaris, Caltha palustris, *Dryas octopetala, Empetrum nigrum, Ephedra, Helianthemum, Hippophaë rhamnoides, Juniperus, Plantago, Polygonum, Populus tremula, Rumex, *Salix polaris, *S. reticulata, *S. herbacea, Saxifraga, Urtica*
14.1 – 12.7 ka BP	*Artemisia, Astralagus alpinus, *Betula nana, *Betula pubescens, Calluna vulgaris, Cerstium alpinum, *Dryas octopetala, Dryopteris, *Empetrum nigrum, Ephedra, Helianthemum, Hippophaë, Isoëtes, Jasione montana, *Juniperus communis, Lycopodium, Lastrea, Myriophyllum alterniflorum, Plantago, Polygonum, Populus tremula, Potentilla palustris, Prunus padus, Pimpinella, Polypodium, Ranunculus, Rubus, *Salix polaris, *S. reticulata, *S. herbacea, Sanguisorba, Sorbus, Saxifraga, Typha latifolia, Urtica, Valeriana officinalis*
12.7 – 11.7 ka BP	*Artemisia, Astralagus alpinus, *Betula nana, Calluna vulgaris, Cerstium alpinum, Chamaenerion alpinum, *Dryas octopetala, Dryopteris, Empetrum nigrum, Ephedra, Helianthemum, Hippophaë, Jasione montana, *Juniperus communis, Lycopus europaeus, Lycopodium, Lastrea, Minuartia, Myriophyllum alterniflorum, M. spicatum, M. verticillatum, Oxytropis capestris, Oxyria digyna, *Pinus sylvestris, Plantago, Polygonum, Potentilla palustris, Populus tremula, Ranunculus, Rumex acetosella, Rubus, *Salix polaris, *S. reticulata, *S. herbacea, Sanguisorba, Sorbus, Saxifraga, Selaginella selaginoides, Urtica*
11.7 – 10 ka BP	*Artemisia, Astralagus alpinus, *Betula nana, Botumus umbellatus, Calluna vulgaris, Cerastium alpinum, Chamaenerion augustifolium, Caltha palustris, *Dryas octopetala, Dryopteris, Empetrum nigrum, Ephedra, Helianthemum, *Hippophaë, Isoëtes lacustris, *Juniperus communis, Littorella uniflora, Lycopodium, Lastrea, Menyanthes trifoliata, Myriophyllum alterniflorum, M. spicatum, M. verticillatum, *Pinus sylvestris, Polygonum, Populus tremula, Ranunculus, Rumex acetosella, Rubus fruticosus, Sanguisorba, Sorbus, *Salix polaris, *S. reticulata, Saxifraga, Typha latifolia, Urtica*

Table 7. Revised time scale for southern Sweden's regional Lateglacial pollen
zones (Björck & Möller 1987) based on Hässeldala Port's pollen stratigraphies
(Andersson 2004; Karlatou-Charampopoulou 2016) and chronology.

Regional pollen zone	Age assignment (cal. ka BP)
Younger Dryas/Preboreal transition zone	11.85-11.58
Younger Dryas	12.54-11.85
Alleröd/Younger Dryas transition zone	12.77-12.54
Alleröd II	13.24-12.77
Alleröd I	14.06-13.24
Older Dryas	>14.06